



AMERICAN METEOROLOGICAL SOCIETY

Journal of the Atmospheric Sciences

EARLY ONLINE RELEASE

This is a preliminary PDF of the author-produced manuscript that has been peer-reviewed and accepted for publication. Since it is being posted so soon after acceptance, it has not yet been copyedited, formatted, or processed by AMS Publications. This preliminary version of the manuscript may be downloaded, distributed, and cited, but please be aware that there will be visual differences and possibly some content differences between this version and the final published version.

The DOI for this manuscript is doi: 10.1175/JAS-D-17-0182.1

The final published version of this manuscript will replace the preliminary version at the above DOI once it is available.

If you would like to cite this EOR in a separate work, please use the following full citation:

Johnson, R., and P. Ciesielski, 2017: Multiscale Variability of the Atmospheric Boundary Layer during DYNAMO. *J. Atmos. Sci.* doi:10.1175/JAS-D-17-0182.1, in press.

© 2017 American Meteorological Society



1 **Multiscale Variability of the Atmospheric Boundary Layer**

2 **during DYNAMO**

3 Richard H. Johnson*, and Paul E. Ciesielski

4 *Department of Atmospheric Science, Colorado State University, Fort Collins, Colorado*

PRELIMINARY ACCEPTED VERSION

5 * *Corresponding author address:* Richard H. Johnson, Department of Atmospheric Science, 1371

6 Campus Delivery, Colorado State University, Fort Collins, CO 80523.

7 E-mail: johnson@atmos.colostate.edu

ABSTRACT

8 Properties of the atmospheric boundary layer (ABL) over the central Indian
9 Ocean are investigated using sounding data obtained during the Dynamics of
10 the MJO (DYNAMO) field campaign in 2011-12. Observations from Gan
11 Island on Addu Atoll, the R/V *Revelle*, and Malé in the Maldives are used
12 to determine the frequency of well-mixed layers, as well as their mean ther-
13 modynamic and wind profiles. Well-mixed boundary layers or mixed layers
14 were observed 68% of the time from the three sites, ranging from ~ 100 -m
15 depth in recovering convective downdraft wakes to ~ 925 m in undisturbed
16 conditions, with a mean depth of 508 m. At *Revelle*, the site most represen-
17 tative of the open ocean, the ABL displayed a distinct signal of modulation
18 by the October and November MJOs, with mixed layer depths gradually in-
19 creasing through the suppressed phases as the sea surface temperature (SST)
20 increased leading up to the active phases, followed by frequent ABL stabiliza-
21 tion and shallow mixed layers in recovering wakes. A distinct diurnal cycle of
22 mixed layer depths and properties was observed during the MJO suppressed
23 phases in response to a diurnal cycle of the SST under the mostly light-wind,
24 clear-sky conditions. The daytime growth of the mixed layer contributed to
25 an afternoon maximum in cumulus cloud development and rainfall during the
26 suppressed periods by allowing more boundary layer thermals to reach their
27 condensation levels. The variability of the ABL on time scales ranging from
28 convective to diurnal to monthly poses significant challenges for numerical
29 simulations of the MJO and the tropical circulation in general.

30 **1. Introduction**

31 A major challenge in numerical weather and climate prediction is the realistic treatment of the at-
32 mospheric boundary layer (ABL) (Teixeira et al. 2008). Complicating factors include the coupling
33 of the boundary layer with the underlying surface, stratification effects, surface inhomogeneities,
34 complex turbulent structures, intermittency, non-local mixing, etc. An additional difficulty, par-
35 ticularly in the tropics, is the coupling of the ABL with the cloud layer, including boundary layer
36 modification by convective clouds and precipitation. The challenge extends well beyond individ-
37 ual clouds to organized convective systems across a wide span of time scales, from mesoscale
38 convective systems to equatorial waves to the Madden-Julian Oscillation (MJO). The recent DY-
39 NAMO (Dynamics of the MJO)¹ field campaign (Yoneyama et al. 2013; Zhang et al. 2013) affords
40 a unique opportunity to investigate the multiscale variability of the boundary layer under a wide
41 range of convective activity throughout the life cycle of the MJO.

42 Surface, sounding, and radar measurements collected during DYNAMO have shed new light
43 on properties of the boundary layer and lower troposphere from the suppressed to active phases
44 of the MJO. During suppressed periods, boundary layer circulations frequently developed that
45 brought about organized roll and cellular patterns of shallow convection and played a role in lower-
46 tropospheric moistening (Bellenger et al. 2015; Rowe and Houze 2015; Ruppert and Johnson 2015,
47 2016). Despite the shallowness and scattered nature of convection during these times, evaporation
48 from precipitating clouds generated distinct cold pools that modified near-surface wind and ther-
49 modynamic conditions (Chen et al. 2016; de Szoeke et al. 2017), contributing to further convective
50 cloud development (Rowe and Houze 2015; Feng et al. 2015). Proceeding into the active phase,

¹The field campaign consisted of four collaborating components: DYNAMO, CINDY (Cooperative Indian Ocean experiment on intraseasonal variability in the Year 2011), AMIE (ARM MJO Investigation Experiment), and LASP (Littoral Air-Sea Processes). We will refer to the combined effort as DYNAMO.

51 the frequency of cold pools increased (Moum et al. 2014; de Szoeke et al. 2017) associated with
52 increased rainfall and more numerous mesoscale convective systems (Xu and Rutledge 2014). The
53 characteristics of the convectively generated cold pools over the Indian Ocean during DYNAMO
54 bear close resemblance to those previously observed in field campaigns over the tropical Atlantic
55 (Houze 1977; Zipser 1977; Barnes and Garstang 1982; Johnson and Nicholls 1983; Jorgensen
56 et al. 1997; Zuidema et al. 2012) and the tropical western Pacific (Young et al. 1995; Saxen and
57 Rutledge 1998).

58 While the evolution of surface wind and thermodynamic properties, surface fluxes, upper ocean
59 structure, clouds, and precipitation fields over the life cycle of the DYNAMO MJOs have been
60 documented in a number of recent studies (Johnson and Ciesielski 2013; Powell and Houze 2013,
61 2015b; Moum et al. 2014; Xu and Rutledge 2014; de Szoeke et al. 2015, 2017; Baranowski et al.
62 2016), the variability of the atmospheric mixed layer during DYNAMO has yet to be fully ex-
63 plored. In an investigation for a limited period of DYNAMO, Chen et al. (2016) found using air-
64 craft dropsonde data that the height of the atmospheric boundary layer was ~ 100 m greater during
65 the suppressed phase of the November DYNAMO MJO than during the convectively active phase.
66 This observation is consistent with the findings of Johnson et al. (2001) who used sounding data
67 from the Tropical Ocean Global Atmosphere Coupled Ocean-Atmosphere Response Experiment
68 (TOGA COARE) to investigate the multiscale variability of the mixed layer for that experiment.
69 It was found that well-mixed layers were observed about two-thirds of the time during COARE,
70 ranging from as high as 960-m depth during periods of dry intrusions over the warm pool to as
71 shallow as ~ 100 -200 m in recovering downdraft wakes. In addition, a diurnal variation in the
72 mixed-layer depth was observed on undisturbed, light-wind days during the suppressed phase of
73 the December 1992 MJO when a diurnal cycle in sea surface temperature (SST) up to 2 - 3°C ex-
74 isted.

75 It is becoming increasingly clear that a realistic representation of the boundary layer throughout
76 the life cycle of the MJO is important for successful numerical simulations of the phenomenon.
77 The sensitivity of simulations of the MJO to the treatment of the boundary layer was recently
78 demonstrated by Qian et al. (2016), who showed using the Weather Research and Forecasting
79 (WRF) model that the simulated precipitation and surface moisture fluxes over the Indian Ocean
80 during DYNAMO exhibited “surprising large” differences with the application of various bound-
81 ary layer parameterization schemes. These authors compared simulated boundary layer properties
82 to those observed by soundings taken at Addu Atoll (Gan Island) and found significant differences
83 in the profiles of virtual potential temperature, moisture, and moist static energy extending from
84 the surface up to 5 km for the different boundary layer schemes used.

85 A further complication to boundary layer treatment in MJO simulations is the proper represen-
86 tation of diurnal cycle effects. A substantial diurnal cycle in SST was observed during the DY-
87 NAMO suppressed phases (Matthews et al. 2014; Chen et al. 2015; Ruppert and Johnson 2015),
88 which presumably impacts the diurnal cycle of the atmospheric mixed layer, as was shown to be
89 the case for COARE (Johnson et al. 2001). The SST diurnal cycle appears to be important for
90 realistic model representation of lower tropospheric moistening during the preonset phase of the
91 MJO (Seo et al. 2014; Ruppert and Johnson 2016).

92 The present study aims to utilize the extensive DYNAMO sounding dataset to determine the
93 multiscale variability of the atmospheric mixed layer over the Indian Ocean during that experi-
94 ment, and compare the findings to those for COARE reported in Johnson et al. (2001). There
95 are several advantages of the DYNAMO dataset over COARE for study of the mixed layer. First,
96 there were three prominent MJOs during DYNAMO (in October, November, and December) as
97 opposed to a single distinct event in COARE. Secondly, the higher time resolution of soundings (3-
98 hourly) during DYNAMO is superior for determining the diurnal cycle of the mixed layer than the

99 6-hourly soundings during COARE. Finally, there have been significant improvements in the ra-
100 diosonde humidity sensors used during DYNAMO over those used twenty years earlier in COARE
101 such that humidity sensor errors have been much reduced (Ciesielski et al. 2014).

102 **2. Data and Methods**

103 *a. Data*

104 Mixed layer properties are determined from the radiosonde measurements taken from the DY-
105 NAMO sounding arrays. The DYNAMO sounding network consisted of two quadrilateral arrays,
106 one north and one south of the equator (Fig. 1). Details of the sounding systems, observing char-
107 acteristics, and sounding data quality-control procedures are contained in Ciesielski et al. (2014).
108 As indicated by the MJO amplitude shown in Fig. 1 and reported in Johnson and Ciesielski (2013),
109 the strongest MJO signal occurred over the northern sounding array, as opposed to the southern
110 array. Therefore, for the purposes of this study, mixed layer properties are examined at the three
111 sites Gan Island, Malé, and the R/V *Revelle* in Fig. 1. Soundings from Malé were at 6-hourly in-
112 tervals, while those at Gan and *Revelle* were at 3-hourly intervals. The October-November period
113 of DYNAMO was designated the Special Observing Period (SOP); however, the sounding arrays
114 were intact for the majority of the time between 1 October and 15 December, so we will refer
115 to the latter period as the SOP. Soundings from Colombo, Sri Lanka, were heavily influenced by
116 local island effects, so that site is excluded from the mixed layer analysis.

117 Soundings at Gan Island, Malé, and *Revelle* used Vaisala RS92 systems. The humidity data have
118 been corrected following the procedures outlined in Ciesielski et al. (2014). The corrected RS92
119 humidity data had a slight nighttime moist bias ($\sim 1\%$) in the lower troposphere, considerably less

120 than that of the RS80 sensors used in COARE. Surface data points for the soundings were from
121 meteorological sensors at 2 m at Gan Island and Malé and 19 m at *Revelle*.

122 Surface fluxes and SST were obtained from in situ measurements onboard the R/V *Revelle*, made
123 available via <ftp://dynamo.dms.uconn.edu/> through a collaborative effort between NOAA/Physical
124 Sciences Division/ESRL, Oregon State University, and the University of Connecticut. Bulk fluxes
125 were computed using the COARE 3.0 algorithm (Fairall et al. 2003).

126 Rainfall rates at Gan and *Revelle* are based on the National Center for Atmospheric Re-
127 search (NCAR) S-Polka and Tropical Ocean Global Atmosphere (TOGA) radar estimates,
128 respectively, obtained from the DYNAMO Data Legacy Project website [http://dynamo.fl-
129 ext.ucar.edu/rsmas/dynamo_legacy/](http://dynamo.fl-ext.ucar.edu/rsmas/dynamo_legacy/). The radar estimates for Gan and *Revelle* are 10-min averages
130 over a 320 km \times 320 km area surrounding each site. Images of PPI scans from the TOGA radar
131 aboard the *Revelle* are from <http://catalog.eol.ucar.edu/dynamo/>. Terra/MODIS satellite images
132 have been obtained from <https://lance3.modaps.eosdis.nasa.gov/cgi-bin/imagery/realtime.cgi>.
133 Rainfall at the three sites was also estimated from the 3-h, 0.25° resolution TRMM 3B42v7
134 rainfall product (Huffman et al. 2007). Cloud cover estimates were based on ceilometer obser-
135 vations at *Revelle*. Cloud coverage for the November suppressed period was defined from 1-h
136 ceilometer data as the fraction of the time clouds were overhead. Vertical motion field used
137 in constructing Fig. 1 was from the V3b Colorado State University gridded analysis product at
138 <http://johnson.atmos.colostate.edu/dynamo/products/gridded/index.html>.

139 *b. Mixed layer depth analysis*

140 Mixed layers are commonplace over the tropical ocean, characterized by a layer \sim 500-600 m
141 deep of nearly constant potential temperature θ (e.g., Malkus 1958; LeMone and Pennell 1976;
142 Fitzjarrald and Garstang 1981; Johnson et al. 2001). Specific humidity q in mixed layers ranges

143 from being a constant to gradually decreasing with height through its depth by $0.5\text{-}1\text{ g kg}^{-1}$. This
144 decrease is a result of dry air entrainment into the mixed layer, as reflected by large variances
145 in q in the upper part of the mixed layer (e.g., Nicholls and LeMone 1980). The mixed layer is
146 typically capped by an entrainment zone $\sim 50\text{-}150$ m deep containing sharp vertical gradients in θ
147 and q . During periods of precipitation, cool downdraft outflows often stabilize the boundary layer,
148 followed by a recovery period with deepening mixed layers lasting from a few hours up to a half
149 day or longer (e.g., Zipser 1977; Young et al. 1995; Jorgensen et al. 1997; Chen et al. 2016).

150 A variety of objective techniques have been developed to determine the depth of the atmospheric
151 boundary layer (ABL) under stratifications ranging from convectively unstable, neutral, to stable.
152 Mixed layers commonly exist under unstable and neutral conditions. The techniques used, how-
153 ever, often lead to different ABL and mixed-layer depth estimates (e.g., Liu and Liang 2010; Seidel
154 et al. 2010; Wang and Wang 2014). Recognizing these difficulties, and drawing upon experience
155 from COARE (Johnson et al. 2001), we use the subjective procedure employed in that study for
156 identification of mixed layers and determination of their depths and properties, which is described
157 next.

158 Soundings from Malé, Gan, and *Revelle* (Fig. 1) are identified as having mixed layers if the
159 following conditions are met: θ is approximately constant with height from the surface (or the
160 top of a superadiabatic layers when it exists) up to a height z_i , the mixed layer top, with an abrupt
161 increase in stability above z_i ; and q is constant or decreases only slightly from the surface up to z_i
162 and then decreases rapidly above. The vertical resolution of the sounding data used in the analysis
163 is 5 hPa, which roughly corresponds to 50 m in the boundary layer. Since the true z_i may not
164 correspond exactly with one of the 5-hPa pressure levels, a sounding is designated as having a
165 mixed layer if it is determined that a mixed layer exists for *both* θ and q and the values of z_i for
166 each agree within 5 hPa of each other. The value of z_i assigned for the sounding is based on which

167 θ or q profile best depicts a well-mixed structure. An entrainment zone ~ 50 -150 m deep having
168 a base at z_i was observed for many of the mixed layers. Although the top of the entrainment
169 zone was not determined in our analysis, its existence shows up in plots of the thermodynamic
170 properties of mixed layer scaled by mixed layer depth that are presented later.

171 A complication with determination of mixed layer properties from Gan and Malé is the fact that
172 the soundings were taken over land adjacent to airport runways. Given the well-known heating
173 effect of islands (e.g., Malkus and Stern 1953), the lowest part of soundings is often modified from
174 the structure that exists over the adjacent open ocean. The Malé observation site was on Velana
175 International Airport portion of Hulhule Island, a strip of land approximately 500 m wide and
176 3000 m long. The Gan observation site was on Addu Atoll, a much larger island with an enclosed
177 shallow lagoon approximately 5 km across. The heat source represented by Addu Atoll clearly has
178 the potential of influencing the boundary layer properties given by the Gan soundings. The smaller
179 dimension of Malé than Gan argues for a smaller heat island effect there; nevertheless, land effects
180 cannot be ignored in the interpretation of the lowest 50 m of the Malé soundings. The soundings
181 from *Revelle* are the most representative of open ocean conditions, but the ship superstructure no
182 doubt impacted the lowest 50 m or so for some of the soundings.

183 **3. Results**

184 *a. Mean properties of the mixed layer*

185 The focus of the study is on well-mixed boundary layers, which can occur under unstable or
186 neutral conditions. Characteristics of stable layers, other than their frequency of occurrence, are
187 not considered here. Two instances where mixed layers were identified are illustrated in Fig. 2, a
188 plot of soundings from the *Revelle* taken on 4 October during the suppressed phase of the MJO.

189 Profiles of θ and q are approximately well mixed up to about 500 m, surmounted by an entrainment
190 zone ~ 100 m deep featuring sharp increases in stability and strong drying. Although not the focus
191 of our study, the figure depicts an hypothesized trade-wind-like cumulus layer, capped by a slightly
192 more stable layer and increased moisture lapse rate (Malkus 1958; Augstein et al. 1974). This
193 illustration provides a broader context for the types of conditions observed during the suppressed
194 phases of the MJO. In support of this depicted structure, the Terra/MODIS visible image in Fig.
195 2 shows scattered cumulus patches in the area of the *Revelle* around the time of the soundings.
196 Similar trade-wind-like conditions during the suppressed phase of the MJO were observed during
197 COARE (Johnson and Lin 1997).

198 As previously mentioned, an advantage of having 3-hourly soundings is the ability to better
199 resolve the diurnal cycle of the mixed layer. However, this time resolution also allows for an
200 improved sampling over that during COARE of the recovery of the mixed layer following deep
201 convection. As an illustration, soundings at 3-hourly intervals from the *Revelle* on 22 November
202 (Fig. 3) show the stabilization of the boundary layer around 0200 UTC (0700 L) by precipitation
203 systems detected by the TOGA radar at 0229 UTC. Over the following 12 hours, the mixed layer
204 deepened from 985 hPa (230 m) at 1000 L (0500 UTC) to 970 hPa (360 m) at 1900 L (1400
205 UTC) as the precipitation waned. This lengthy recovery period is consistent with some of the
206 DYNAMO cases reported by Chen et al. (2016) using aircraft data to determine recovery times
207 and is not unlike findings from past studies (Houze 1977; Zipser 1977; Fitzjarrald and Garstang
208 1981; Johnson and Nicholls 1983; Jorgensen et al. 1997).

209 An inventory of sounding classifications for all three sites is provided in Table 1. An average
210 of 68% (ranging from 64 to 72%) of the 1783 soundings in DYNAMO exhibited mixed layer
211 structures, slightly less than the 72% reported by Johnson et al. (2001) for soundings analyzed in
212 COARE. These percentages are also somewhat less than the 79.5% frequency of mixed layers that

213 Fitzjarrald and Garstang (1981) determined using the Boundary Layer Instrumentation System in
214 the GARP Atlantic Tropical Experiment (GATE). Table 1 shows that stable layers, which princi-
215 pally occurred during periods of precipitation, existed on average about 12% of the time, while the
216 remaining soundings (17%) had indeterminate profiles, i.e., they were not stable, but a well-mixed
217 structure could not be identified.

218 Mean properties of the mixed layers at the three sites for the SOP are shown in Table 2, along
219 with comparisons with COARE and GATE results. The mean mixed layer depth \bar{z}_i for the three
220 sites in DYNAMO is 508 m. The ranking of mean depths from highest to lowest, 535 m at Malé
221 to 503 m at Gan to 491 m at *Revelle*, is the reverse of the ranking of rainfall rates and frequency of
222 rainfall at the three sites (Table 2). Namely, shallower mean mixed layer depths occurred with the
223 greater rainfall rates and rainfall frequencies, implying the more frequent recovering precipitation
224 downdraft wakes. The large standard deviations (146-171 m) of z_i reflect the existence of numer-
225 ous mixed layer modifying processes: convective downdrafts from isolated showers all the way
226 up to mesoscale convective systems, westerly wind bursts, organized boundary layer circulations
227 such as rolls and open cells, and the diurnal cycle. The mean z_i of 508 m for DYNAMO is in
228 close agreement with the 512 m mean value for COARE (Johnson et al. 2001) based on a nearly
229 equal number of cases, but is somewhat greater than the GATE mean value of 424 m obtained by
230 Fitzjarrald and Garstang (1981).

231 Histograms of mixed layer depths (Fig. 4) show similar distributions and a wide range of values
232 at all sites during DYNAMO. Using a chi-square test, the distributions are found to be normal or
233 Gaussian at the 0.05 significance level. However, each has negative skewness, reflecting the effects
234 of convective downdraft wakes and shallow mixed layers during the recovery process. To illus-
235 trate the role of precipitation influence on mixed layer depth, a histogram of mixed layer depths for
236 undisturbed and disturbed periods using the full record of soundings (1 October to 8 February) at

237 Gan during DYNAMO is shown in Fig. 5. Undisturbed periods are defined according to Ruppert
238 and Johnson (2015) as suppressed and “bottom-heavy” heating periods, while disturbed periods
239 are defined as periods with “top-heavy” heating rates. This division of periods reflects the verti-
240 cal growth of convection into the active phase of the MJO while at the same time a progression
241 towards increasing areal coverage of convective downdrafts and their initially shallow but recov-
242 ering wakes. There are stark differences in the distributions, with a single peak at upper levels
243 on undisturbed days and several peaks (perhaps due to the smaller sample size) at lower levels on
244 disturbed days. The mean z_i on undisturbed days is 559 m, while 422 m on disturbed days.

245 Figure 6 shows the mean wind and thermodynamic properties in the mixed layer for all three
246 sites. To make the comparisons contemporaneous, soundings were included for only those times
247 when the *Revelle* was on station at its equatorial location. In order to preserve mixed layer struc-
248 tures, variables in each sounding are first scaled by mixed layer depth z_i , then composited accord-
249 ing to height relative to z_i , and finally replotted unscaled such that the mean values of z_i for each
250 site are appropriately shown. Sounding data in the lowest 50 m are shaded to indicate a region of
251 varying surface effects. Mean profiles of θ , virtual potential temperature θ_v , and q are nearly well
252 mixed at all three sites, though θ is about 0.5 K cooler at Gan than at Malé or *Revelle*. Although
253 data are not scaled relative to the depth of the entrainment zone, its existence is evident in most
254 of the composite profiles by changes in stability and lapse rate of $q \sim 50\text{-}100$ m above z_i . It is
255 unclear why Gan is slightly cooler than *Revelle*, in particular, since the latter location is slightly
256 rainier (Table 1) and the mean SST during DYNAMO at all three sites is approximately the same
257 (Johnson and Ciesielski 2013). Moreover, the Gan sounding site is along a runway, so it is not
258 obvious why the mixed layer should be cooler there. With respect to q , the fact that *Revelle* is
259 slightly moister makes sense since it is a rainier location. Wind speeds in the mixed layers are
260 about the same throughout much of their depths ($\sim 5 \text{ m s}^{-1}$), though Gan and Malé are slightly

261 calmer in the lowest 200 m due to island/atoll frictional effects. The mixed layer properties shown
262 in Fig. 6 closely resemble those found by Fitzjarrald and Garstang (1981) for GATE and Johnson
263 et al. (2001) for COARE.

264 To characterize the properties of the mixed layers more fully, CFADs (contoured frequency
265 by altitude diagrams; Yuter and Houze 1995) of mixed-layer mean θ , q , and TOGA-radar rainfall
266 within 3 h of sounding observation time at *Revelle* were constructed (Fig. 7). Shallow mixed layers
267 were cooler and moister (higher q) than deep mixed layers as a result of precipitation downdrafts
268 associated with higher rainfall rates. Deep mixed layers most often occurred under non-rainy con-
269 ditions as indicated by radar-determined rainfall (except for an isolated peak near 20 mm day^{-1})
270 and are warm and dry, their properties being more characteristic of suppressed MJO conditions.

271 *b. Mixed layer variability for full DYNAMO period*

272 Mixed layer depths at all three sites for the full duration of DYNAMO are shown in Fig. 8,
273 along with time series of rainfall P_0 and precipitable water PW. The observations at Gan extend
274 into early February, well beyond the SOP operations at Malé and *Revelle*. The late October and
275 late November rainy periods, roughly corresponding to MJO phases 2 and 3 based on Wheeler
276 and Hendon (2004) index (bottom bar in Fig. 8), were associated with two MJOs that occurred
277 during DYNAMO (Gottschalck et al. 2013; Yoneyama et al. 2013). PW at Gan and *Revelle* in-
278 creased after a dry period during the first week of October, followed by the onset of rainfall and
279 a reduction in mixed layer depths, most notably at *Revelle*, reflecting the effects of recovering
280 convective downdraft wakes (e.g., Fitzjarrald and Garstang 1981). The moistening and rain onset
281 at Malé, along with reduction in mixed layer depths, began about one week later as the envelope
282 of convection from the southern hemisphere gradually shifted northward across the equator (Fig.
283 8, Johnson and Ciesielski 2013). Decreased mixed layer depths were also observed at *Revelle* and

284 Malé in the last half of November with the second MJO. While there is some reduction in mixed
285 layer depths at Gan during the MJO active phases, this behavior is not as prominent as the other
286 sites. The reason for the lack of a distinct modulation of mixed layer depths by the MJOs at Gan is
287 not obvious. However, a possible explanation lies in the fact that with an enclosed lagoon, Addu
288 Atoll represents a relatively large heat source impacting the lowest levels of the Gan soundings,
289 hence making them less representative of open-ocean conditions and more dependent on the local
290 diurnal cycle of heating. A prominent feature of the time series at Gan is the extended period of
291 deeper mixed layers during the dry period in January and early February. Mean mixed-layer depths
292 during this time were consistently greater, ~ 600 m, typical of undisturbed trade-wind conditions
293 (Malkus 1958; Augstein et al. 1974).

294 Considering that *Revelle* soundings are most representative of open-ocean conditions and that in
295 situ flux measurements were made at that location, further analysis of the mixed layer evolution
296 is carried out for that site. Time series of the mixed layer depths and companion fields based on
297 *Revelle* data during the DYNAMO SOP are shown in Fig. 9. All curves are daily-average values
298 except z_i and SST, which are at their full measured resolution. The first twelve days of October, a
299 suppressed MJO period over the Indian Ocean (MJO phases 6, 7, and 8), were marked by steadily
300 increasing mixed layer depths to over 800 m, increasing SST and near-surface (19 m) temperature
301 T_{19m} , relatively low surface relative humidity RH, and little rainfall (Fig. 9a,c,d). The SST exhibits
302 a diurnal cycle throughout the October suppressed period despite moderate surface wind speeds
303 of $4\text{-}6\text{ m s}^{-1}$ (Fig. 9b). The amplitude of the SST diurnal cycle was greater in early November
304 due to the lighter winds then (Ruppert and Johnson 2015). The diurnal cycle during both periods
305 generated an afternoon maximum in shallow cumulus clouds, often organized in rolls or open cell
306 patterns, that played a role in lower-tropospheric moistening in the preonset stages of the MJOs
307 (Ruppert and Johnson 2015; Rowe and Houze 2015).

308 Also shown in Fig. 9a is the daily-averaged lifting condensation level (LCL) based on the mean
309 thermodynamic properties of the mixed layer. During the first twelve days of October, LCL and z_i
310 rose commensurately, with z_i reaching the LCL on a number of occasions and eventually exceeding
311 it late in the period when the deepest mixed layers occurred. While the LCL curve represents
312 daily-averaged values and z_i is at 3 h intervals (the diurnal cycle of LCL will be examined later),
313 the results broadly suggest that boundary layer thermals during the suppressed period can often
314 reach the LCL and form cumulus clouds, especially toward the end of the period. This result is
315 consistent with observations of shallow clouds being prevalent during the suppressed period, with
316 increasing cloud amount toward the end of it (Ruppert and Johnson 2015; Rowe and Houze 2015).
317 The *Revelle* was off station in early November at the beginning of the second suppressed period,
318 but towards the end of this period up to about the 18th, z_i was near or greater than LCL on a number
319 of occasions. Therefore, through the suppressed phase of both MJOs, cumulus cloud populations
320 were aided by deeper mixed layers permitting boundary layer thermals to reach their condensation
321 levels and promote shallow cumulus development. Since the horizontally homogeneous, steady-
322 state mixed layer depth over the ocean is directly proportional to the surface buoyancy flux F (= $\rho c_p \overline{w'\theta'_v}$)
323 and inversely related to the magnitude of the large-scale subsidence (e.g., Johnson et al.
324 2001), the fact that F is approximately constant during the first twelve days of October suggests
325 that the deepening mixed layers during that period could be related to a relaxation of large-scale
326 subsidence. Powell and Houze (2015a) argued that such a situation occurred in association with
327 the arrival of global-circumnavigating, upper-tropospheric velocity potential anomalies over the
328 Indian Ocean. The reduction in subsidence through the suppressed phase is also consistent with
329 results reported in Sobel et al. (2014) and Johnson et al. (2015) of decreasing net-tropospheric
330 radiative cooling rates (implying weaker large-scale subsidence) linked to gradually increasing

331 cirrus clouds shown in the latter paper during the buildup to the active phases of both the October
332 and November MJOs.

333 Surface wind speed and buoyancy flux $F (= \rho c_p \overline{w' \theta'_v})$ at the *Revelle* increased significantly
334 during the active phases of the October and November MJOs (Fig. 9b). Frequent cold pools were
335 observed during these periods (de Szoeke et al. 2017), which contributed to the enhanced surface
336 sensible and latent heat fluxes (Johnson et al. 2015) and the recovery of convective outflow wakes
337 as evidenced by the numerous shallow mixed layers (Fig. 9a).

338 *c. Mixed layer diurnal cycle during undisturbed conditions*

339 The diurnal cycle of the SST and its impact on cumulus convection were prominent features of
340 the MJO suppressed phases during DYNAMO (Matthews et al. 2014; Ruppert and Johnson 2015).
341 Therefore, we give attention to suppressed or undisturbed periods for the study of the mixed layer
342 diurnal cycle. In a previous investigation using 6-hourly COARE sounding data, a mixed layer
343 diurnal cycle was observed during undisturbed, light-wind conditions (Johnson et al. 2001). At
344 R/V *Shiyan 3* a diurnal cycle in SST of 1-2°C produced a diurnal cycle in mixed layer properties:
345 a 60 m increase in z_i in the afternoon accompanied by a 0.5 K warming and 0.5 g kg⁻¹ drying.
346 The SST diurnal cycle at the ship was muted on disturbed days by strong winds and precipitation
347 downdrafts. Here we report similar observations from DYNAMO, though the diurnal cycle is
348 much better resolved with the 3-hourly soundings at Gan and *Revelle*.

349 Figure 10 shows SOP-undisturbed-mean diurnal cycle in z_i and mixed-layer mean values of θ
350 and q at all three sounding locations, as well as SST at *Revelle*. The undisturbed periods approx-
351 imately correspond to the suppressed SOP periods defined in Ruppert and Johnson (2015). All
352 three sites show a diurnal cycle in z_i of 100-150 m peaking in the afternoon at Gan and *Revelle* and
353 near midnight at Malé (Fig. 10a), though the timing of the true maximum for the latter site is less

354 certain due to the 6-hourly time resolution. Each site shows an afternoon mixed layer warming
355 ~ 0.5 K and drying of ~ 0.5 g kg⁻¹. The warming is in part attributed to a diurnal warm layer that
356 develops in the upper ~ 1 m of the ocean under under light-wind, clear-sky conditions (Soloviev
357 and Lukas 1997; Vialard et al. 2009; Moum et al. 2014), as reflected by the SST diurnal cycle
358 shown in Figs. 9c and 10d. Enhanced surface fluxes from this upper ocean warming served to
359 warm the mixed layer (Fig. 10b) and contributed to an afternoon maximum in the cumulus cloud
360 population (Ruppert and Johnson 2015, 2016). Daytime absorption of solar shortwave radiation,
361 primarily by water vapor, has been argued to additionally contribute to daytime heating of the
362 mixed layer (Parsons et al. 2000; Johnson et al. 2001).

363 Mixed layer drying during the daytime (Fig. 10c) is partly a result of the downward entrainment
364 of dry air from above as the mixed layer grows during the day. However, the drier conditions in
365 the daytime may also partly be a reflection of moistening of the boundary layer over the equa-
366 torial oceans that occurs at night due to radiative and/or larger-scale circulation processes (Sui
367 et al. 1997; Bellenger et al. 2010). The mixed layer at Malé is the driest of the three sites, likely
368 due to its off-equatorial, northern hemisphere location, while *Revelle* has the highest q (Fig. 10c).
369 The moister conditions at *Revelle* are attributed to the fact that it virtually represents open-ocean
370 conditions. Evidence for drier conditions near the surface over land was provided in an inde-
371 pendent study (Todd Jones and Hiroyuki Yamada, 2011, personal communication) where near-
372 simultaneous humidity measurements at the Malé sounding site and the adjacent ocean showed
373 the specific humidity to be ~ 1 g kg⁻¹ greater over water than that over land despite the small area
374 of the island.

375 Additional evidence for contrasting near-surface conditions at Gan and Malé in comparison to
376 those at *Revelle* is provided in Fig. 11. Surface temperature and humidity measurements were at 2
377 m at Gan and Malé, and at the 19-m height of the surface meteorological sensor at *Revelle*. During

378 the undisturbed periods, a moderate daytime surface warming of 2-4°C was observed at Gan and
379 Malé under the mostly clear-sky conditions, as expected at their land locations. In contrast, the 19-
380 m temperature at *Revelle* had a relatively minor diurnal cycle, more accurately reflecting conditions
381 over the open ocean. The diurnal cycle of near-surface specific humidity differed considerably at
382 the three sites. *Revelle* and to a lesser extent Malé showed a midday drying, which may in part
383 have simply been a manifestation of the nocturnal moistening, although the downward mixing of
384 dry air from above the mixed layer may also have contributed to the drying. On the other hand,
385 Gan exhibited a midday moistening of nearly 1 g kg⁻¹. This feature is hard to fully explain, but
386 it may have been a consequence of the sea breeze advecting in moister air from the ocean and
387 lagoon adjacent to Gan Island. At all three sites there was an afternoon minimum in near-surface
388 relative humidity, which was due to the daytime surface heating at Gan and Malé but the daytime
389 reduction in specific humidity at *Revelle*.

390 To further illustrate the diurnal cycle at *Revelle* under undisturbed conditions, a plot of scaled
391 q , θ , and wind speed was created (Fig. 12). Quantities were first scaled by their height relative to
392 mixed layer top at each time, scaled fields were then composited, and lastly values were plotted
393 relative to the mean mixed layer depth at each time. The number of soundings going into the means
394 at each time are shown in Fig. 13a.² Owing to the limited number of soundings in the composite,
395 the diurnal variation of z_i (solid black curve in Fig. 12) does not exhibit a smooth diurnal cycle,
396 i.e., there was a reduction in z_i at 1100 L on its climb to the afternoon peak at 1400 L. Potential
397 temperature θ and q were nearly well mixed below z_i , though there was a slight decrease in q and
398 increase in θ near mixed layer top. Mixed layer warming and drying were observed in mid- to late
399 afternoon, though there was also a drying at 0800 L (which is also evident at Gan, Fig 10c). This

²The sounding at 1100 L on 19 November is excluded from the composite owing to the existence of a very shallow mixed layer in a recovering convective downdraft wake following the passage of isolated showers around that time.

400 two-peak structure to the field of q , rather than there being a broad afternoon minimum, is related
401 to the fact that there was a local minimum in the composite z_i at 1100 L. Namely, shallower mixed
402 layers are moister (Fig. 7), which introduced a local maximum in q at 1100 L.

403 Wind speeds generally increased in the mixed layer in the afternoon (Fig. 12), as found during
404 COARE (Johnson et al. 2001), which is a reflection of more vigorous buoyancy-driven turbulence
405 during the daytime. Downward mixing of higher momentum air from above the mixed layer in
406 the afternoon was not important during this period due to the weak lower-tropospheric winds,
407 although it does appear as a prominent feature in a composite of all 268 mixed profiles at *Revelle*,
408 which includes many disturbed, windy days (not shown). Apart from the wind peak at 2300 L,
409 which represents a sampling problem (there were two anomalously windy days out of only three
410 days in the composite at this time (Fig. 13a)), the wind speed variations (maxima at 0500 and 1700
411 L and minimum at 1100 L) in Fig. 12 are similar to those found using sounding data from COARE
412 (Johnson et al. 2001) and are consistent with past studies of the semidiurnal and diurnal harmonics
413 of wind profiler data for COARE (Gutzler and Hartten 1995) and of buoy data from the Pacific
414 (Deser and Smith 1998).

415 A further analysis of the diurnal cycle of the mixed layer during the November undisturbed
416 period at *Revelle* is shown in Fig. 13. During this period z_i had a diurnal range of about 130 m
417 that accompanied a SST diurnal variation of 1 K (Fig. 13a,c). Buoyancy flux F increased in the
418 afternoon in response to both SST and wind speed increase, as shown by Ruppert and Johnson
419 (2015), which directly contributed to the midday growth in z_i , as also found in COARE (Johnson
420 et al. 2001). In response to the midday heating of the upper ocean, there were local maxima
421 in cloud cover and rainfall (Fig. 13b), as discussed in Ruppert and Johnson (2015, 2016) and
422 observed in previous field campaigns (Sui et al. 1997; Bellenger et al. 2010). In addition, the
423 typical nocturnal rainfall maximum (e.g., Gray and Jacobson 1977) was present during this period

424 despite the suppressed conditions. *The two maxima in rainfall approximately coincide with the*
425 *minima in $LCL - z_i$, which is consistent with the idea that these periods are times in which the*
426 *greatest number of boundary layer thermals are able to reach their condensation levels to form*
427 *clouds.* This semidiurnal cycle to the cloud and precipitation occurrence is shown in Fig. 14
428 (adapted from Ruppert and Johnson (2015)) in terms of the S-PolKa radar echo top height and
429 area coverage diurnal cycle for 13-16 November, a subset of the period analyzed in Fig. 13.

430 **4. Summary and conclusions**

431 Atmospheric sounding data from DYNAMO are used to determine mixed layer depths for three
432 sites that experienced the strongest signal of the Madden-Julian Oscillation during the experiment:
433 Gan Island on Addu Atoll, Malé, and the R/V *Revelle*. Mixed layers were defined to be present
434 when well-mixed profiles of both potential temperature θ and specific humidity q , topped by
435 abrupt increasing stability and drying, were observed to exist and the depths determined by both
436 profiles were within 5 hPa of each other. A number of objective techniques have been developed
437 to determine atmospheric boundary layer (ABL) depths in the past; however, they often lead to
438 different ABL and mixed-layer depth estimates (e.g., Liu and Liang 2010; Seidel et al. 2010;
439 Wang and Wang 2014). Recognizing these difficulties, and drawing upon experience from TOGA
440 COARE (Johnson et al. 2001), the subjective procedure used in that study has been applied to
441 DYNAMO sounding data for identification of mixed layers and determination of their depths and
442 properties.

443 The principal findings of this study are as follows:

- 444 • Mixed layers were observed 68% of the time in DYNAMO (1220 out of 1783 soundings),
445 which is comparable to the 72% frequency found in COARE (Johnson et al. 2001) but some-
446 what less than the 79% frequency determined for GATE (Fitzjarrald and Garstang 1981).

- 447 ● The mean mixed layer depth for all three sites during DYNAMO was 508 m, ranging from
448 491 m at *Revelle* (the rainiest site) to 535 m at Malé (the driest site). The mean value is close
449 to that determined for COARE (512 m; Johnson et al. 2001) but is greater than the mean of
450 424 m determined for GATE (Fitzjarrald and Garstang 1981). Mean mixed layer depth at
451 Gan during a highly suppressed period in January and early February was ~600 m, which is
452 typical of undisturbed trade-wind conditions (Malkus 1958; Augstein et al. 1974).
- 453 ● Mixed layer depths ranged from a high of 926 m to a low of 111 m. Very shallow depths were
454 often observed during the recovery of precipitation downdraft wakes, some of which lasted
455 beyond a half day (Chen et al. 2016). The distributions of mixed layer depths were skewed
456 about the mean toward lower heights, reflecting the frequent presence of such wakes.
- 457 ● Time series for the entire period of DYNAMO reveal a significant modulation of mixed layer
458 depths at Malé and *Revelle* by the October and November MJOs, but less so at Gan. During
459 the October and November suppressed MJO periods at the *Revelle*, the mixed layer depth
460 increased as the SST increased, while large-scale subsidence decreased (Johnson and Ciesiel-
461 ski 2013). The decreasing subsidence may be linked to global-circumnavigating upper-
462 tropospheric velocity potential anomalies that approached the Indian Ocean prior to the active
463 phases of the MJOs (Gottschalck et al. 2013; Powell and Houze 2015a) as well as to a reduc-
464 tion in radiative heating rates caused by increasing cirrus clouds preceding the active phases
465 (Sobel et al. 2014; Johnson et al. 2015). Frequent, shallow mixed layer depths occurred dur-
466 ing the active phases of the MJOs.
- 467 ● A prominent diurnal cycle of the mixed layer properties was observed at all three sites during
468 the suppressed phases of the October and November MJOs in response to the development of
469 an upper-ocean diurnal warm layer and resultant increase in buoyancy fluxes during relatively

470 light-wind, and mostly clear-sky conditions. Diurnal ranges of mixed layer depth, mixed-
471 layer mean θ , and mixed-layer mean q were 100-150 m, 0.5 K, and 0.5 g kg^{-1} , respectively.

472 • The diurnal variation of the mixed layer and its relationship to the lifting condensation level
473 (LCL) related directly to the diurnal evolution of the cloud populations during suppressed pe-
474 riods. The afternoon deepening of the mixed layer coincided with the maximum daytime SST
475 and led to a decrease in the distance between the LCL and the mixed layer top. These condi-
476 tions made it more likely for boundary layer thermals to reach their LCL and create clouds.
477 This conclusion is corroborated by a gradual increase in convective radar echo top heights
478 peaking in mid-afternoon and a local rainfall maximum around that time. During predawn
479 hours, the distance between the LCL and the mixed layer top was similarly small, which co-
480 incided with a nocturnal peak in radar echoes and rainfall. The net result was a semidiurnal
481 variation in precipitation during suppressed periods, consistent with findings from previous
482 studies (Sui et al. 1997; Bellenger et al. 2010).

483 The results of this study bear directly on the problem of numerical simulation of the MJO, as
484 well as global circulation modeling in general. Considering that the proper representation of the
485 atmospheric boundary layer in weather and climate models remains a major challenge (Teixeira
486 et al. 2008), it is important to obtain observations of the boundary layer to validate models. With
487 respect to the MJO itself, Qian et al. (2016) found large sensitivities in the simulation of the MJO
488 using different boundary layer parameterizations in the Weather Research and Forecasting (WRF)
489 model. Cumulus clouds have their roots in the mixed layer, so simulating realistic mixed-layer
490 depth and properties is a logical prerequisite for realistic simulations of cloud populations and
491 their precipitation. This paper is intended to provide analyses that can be used for this purpose.

492 *Acknowledgments.* We appreciate the valuable comments of three reviewers, which have led to
493 significant improvements to the paper. We also thank Jennifer Davison in connection with our
494 early collaborations with her on this work. This research has been supported by the National
495 Science Foundation under Grant AGS-1360237 and by the National Oceanic and Atmospheric
496 Administration (NOAA) under grant NA150AR4310177.

497 **References**

- 498 Augstein, E., H. Schmidt, and F. Ostapoff, 1974: The vertical structure of the atmospheric plane-
499 tary boundary layer in undisturbed trade winds over the atlantic ocean. *Boundary-Layer Meteoro-*
500 *rol.*, **6 (1)**, 129–150, doi:10.1007/BF00232480.
- 501 Baranowski, D. B., M. K. Flatau, P. J. Flatau, and A. J. Matthews, 2016: Impact of atmospheric
502 convectively coupled equatorial Kelvin waves on upper ocean variability. *J. Geophys. Res.*,
503 **121 (5)**, 2045–2059, doi:10.1002/2015JD024150.
- 504 Barnes, G. M., and M. Garstang, 1982: Subcloud layer energetics of precipitating convection.
505 *Mon. Wea. Rev.*, **110 (2)**, 102–117, doi:10.1175/1520-0493(1982)110<0102:SLEOPC>2.0.CO;
506 2.
- 507 Bellenger, H., Y. N. Takayabu, T. Ushiyama, and K. Yoneyama, 2010: Role of diurnal warm layers
508 in the diurnal cycle of convection over the tropical Indian Ocean during MISMO. *Mon. Wea.*
509 *Rev.*, **138 (6)**, 2426–2433, doi:10.1175/2010MWR3249.1.
- 510 Bellenger, H., K. Yoneyama, M. Katsumata, T. Nishizawa, K. Yasunaga, and R. Shirooka, 2015:
511 Observation of moisture tendencies related to shallow convection. *J. Atmos. Sci.*, **72 (2)**, 641–
512 659, doi:10.1175/JAS-D-14-0042.1.

513 Chen, S., and Coauthors, 2015: A study of CINDY/DYNAMO MJO suppressed phase. *J. Atmos.*
514 *Sci.*, **72** (10), 3755–3779, doi:10.1175/JAS-D-13-0348.1.

515 Chen, S. S., and Coauthors, 2016: Aircraft observations of dry air, the ITCZ, convective cloud
516 systems, and cold pools in MJO during DYNAMO. *Bull. Amer. Meteor. Soc.*, **97** (3), 405–423,
517 doi:10.1175/BAMS-D-13-00196.1.

518 Ciesielski, P. E., and Coauthors, 2014: Quality controlled upper-air sounding dataset for DY-
519 NAMO/CINDY/AMIE: Development and corrections. *J. Atmos. Oceanic Technol.*, **31**, 741–
520 764, doi:10.1175/JTECH-D-13-00165.1.

521 de Szoeki, S. P., J. B. Edson, J. R. Marion, C. W. Fairall, and L. Bariteau, 2015: The MJO
522 and air-sea interaction in TOGA COARE and DYNAMO. *J. Climate*, **28** (2), 597–622, doi:
523 10.1175/JCLI-D-14-00477.1.

524 de Szoeki, S. P., E. D. Skyllingstad, P. Zuidema, and A. S. Chandra, 2017: Cold pools and their
525 influence on the tropical marine boundary layer. *J. Atmos. Sci.*, **74**, 1149–1168, doi:10.1175/
526 JAS-D-16-0264.1.

527 Deser, C., and C. A. Smith, 1998: Diurnal and semidiurnal variations of the surface wind field
528 over the tropical pacific ocean. *J. Climate*, **11** (7), 1730–1748, doi:10.1175/1520-0442(1998)
529 011<1730:DASVOT>2.0.CO;2.

530 Fairall, C. W., E. F. Bradley, J. E. Hare, A. A. Grachev, and J. B. Edson, 2003: Bulk parame-
531 terization of airsea fluxes: Updates and verification for the coare algorithm. *J. Climate*, **16** (4),
532 571–591, doi:10.1175/1520-0442(2003)016<0571:BPOASF>2.0.CO;2.

533 Feng, Z., S. Hagos, A. K. Rowe, C. D. Burleyson, M. N. Martini, and S. P. de Szoeki, 2015:
534 Mechanism of convective cloud organization by cold pools over tropical warm ocean during

535 the AMIE/DYNAMO field campaign. *J. Adv. Model. Earth Syst.*, **7**, 357–381, doi:10.1002/
536 2014MS000384.

537 Fitzjarrald, D. R., and M. Garstang, 1981: Vertical structure of the tropical boundary layer. *Mon.*
538 *Wea. Rev.*, **109**, 1512–1526, doi:10.1175/1520-0493(1981)109<1512:VSOTTB>2.0.CO;2.

539 Gottschalck, J., P. E. Roundy, C. J. S. III, A. Vintzileos, and C. Zhang, 2013: Large-scale atmo-
540 spheric and oceanic conditions during the 2011-12 DYNAMO field campaign. *Mon. Wea. Rev.*,
541 **141**, 4173–4196, doi:10.1175/MWR-D-13-00022.1.

542 Gray, W. M., and R. W. Jacobson, Jr., 1977: Diurnal variation of deep cumulus convection. *Mon.*
543 *Wea. Rev.*, **105 (9)**, 1171–1188, doi:10.1175/1520-0493(1977)105<1171:DVODCC>2.0.CO;2.

544 Gutzler, D. S., and L. M. Hartten, 1995: Daily variability of lower tropospheric winds over the
545 tropical western pacific. *J. Geophys. Res.*, **100 (D11)**, 22 999–23 008, doi:10.1029/95JD01879,
546 URL <http://dx.doi.org/10.1029/95JD01879>.

547 Houze, R. A., Jr., 1977: Structure and dynamics of a tropical squall-line system. *Mon. Wea. Rev.*,
548 **105**, 1540–1567, doi:10.1175/1520-0493(1977)105<1540:SADOAT>2.0.CO;2.

549 Huffman, G. J., R. F. Adler, D. T. Bolvin, G. Gu, E. J. Nelkin, K. P. Bowman, E. F. Stocker, and
550 D. B. Wolff, 2007: The TRMM multi-satellite precipitation analysis: Quasi-global, multi-year,
551 combined-sensor precipitation estimates at fine scale. *J. Hydrometeor.*, **8**, 33–55, doi:10.1175/
552 JHM560.1.

553 Johnson, R. H., and P. E. Ciesielski, 2000: Rainfall and radiative heating rate estimates
554 from TOGA COARE atmospheric budgets. *J. Atmos. Sci.*, **57**, 1497–1514, doi:10.1175/
555 1520-0469(2000)057<1497:RARHRF>2.0.CO;2.

556 Johnson, R. H., and P. E. Ciesielski, 2013: Structure and properties of Madden-Julian Os-
557 cillations deduced from DYNAMO sounding arrays. *J. Atmos. Sci.*, **70**, 3157–3179, doi:
558 10.1175/JAS-D-13-065.1.

559 Johnson, R. H., P. E. Ciesielski, and J. A. Cotturone, 2001: Multiscale variability of the atmo-
560 spheric mixed layer over the western Pacific warm pool. *J. Atmos. Sci.*, **58 (18)**, 2729–2750,
561 doi:10.1175/1520-0469(2001)058<2729:MVOTAM>2.0.CO;2.

562 Johnson, R. H., P. E. Ciesielski, J. H. R. Jr., and M. Katsumata, 2015: Sounding-based thermody-
563 namic budgets for DYNAMO. *J. Atmos. Sci.*, **72 (2)**, 598–622, doi:10.1175/JAS-D-14-0202.1.

564 Johnson, R. H., and X. Lin, 1997: Episodic trade wind regimes over the western Pacific warm pool.
565 *J. Atmos. Sci.*, **54**, 2020–2034, doi:10.1175/1520-0469(1997)054<2020:ETWROT>2.0.CO;2.

566 Johnson, R. H., and M. E. Nicholls, 1983: A composite analysis of the boundary layer accompa-
567 nying a tropical squall line. *Mon. Wea. Rev.*, **111 (2)**, 308–319, doi:10.1175/1520-0493(1983)
568 111<0308:ACAOTB>2.0.CO;2.

569 Jorgensen, D. P., M. A. LeMone, and S. B. Trier, 1997: Structure and evolution of the 22 february
570 1993 TOGA COARE squall line: Aircraft observations of precipitation, circulation, and sur-
571 face energy fluxes. *J. Atmos. Sci.*, **54 (15)**, 1961–1985, doi:10.1175/1520-0469(1997)054<1961:
572 SAEOTF>2.0.CO;2.

573 LeMone, M. A., and W. T. Pennell, 1976: The relationship of trade wind cumulus distribu-
574 tion to subcloud layer fluxes and structure. *Mon. Wea. Rev.*, **104 (5)**, 524–539, doi:10.1175/
575 1520-0493(1976)104<0524:TROTWC>2.0.CO;2.

576 Liu, S., and X.-Z. Liang, 2010: Observed diurnal cycle climatology of planetary boundary layer
577 height. *J. Climate*, **23 (21)**, 5790–5809, doi:10.1175/2010JCLI3552.1.

- 578 Malkus, J. S., 1958: On the structure of the trade-wind moist layer. *Pap. Phys. Oceanogr. Meteor.*,
579 **13**, 1–47, doi:10.1575/1912/5443.
- 580 Malkus, J. S., and M. E. Stern, 1953: The flow of a stable atmosphere over a heated island, part 1.
581 *J. Meteor.*, **10** (1), 30–41, doi:10.1175/1520-0469(1953)010<0030:TFOASA>2.0.CO;2.
- 582 Matthews, A. J., D. B. Baranowski, K. J. Heywood, P. J. Flatau, and S. Schmidtko, 2014: The
583 surface diurnal warm layer in the Indian Ocean during CINDY/DYNAMO. *J. Climate*, **27** (24),
584 9101–9122, doi:10.1175/JCLI-D-14-00222.1.
- 585 Moum, J. N., and Coauthors, 2014: Air-sea interactions from westerly wind bursts during the
586 November 2011 MJO in the Indian Ocean. *Bull. Amer. Meteor. Soc.*, **95** (8), 1185–1199, doi:
587 10.1175/BAMS-D-12-00225.1.
- 588 Nicholls, S., and M. A. LeMone, 1980: The fair weather boundary layer in gate: The relationship
589 of subcloud fluxes and structure to the distribution and enhancement of cumulus clouds. *J.*
590 *Atmos. Sci.*, **37** (9), 2051–2067, doi:10.1175/1520-0469(1980)037<2051:TFWBLI>2.0.CO;2.
- 591 Parsons, D. B., J.-L. Redelsperger, and K. Yoneyama, 2000: The evolution of the tropical western
592 pacific atmosphere-ocean system following the arrival of a dry intrusion. *Quart. J. Roy. Meteor.*
593 *Soc.*, **126** (563), 517–548, doi:10.1002/qj.49712656307.
- 594 Powell, S. W., and R. A. Houze, 2013: The cloud population and onset of the Madden-Julian
595 Oscillation over the Indian Ocean during DYNAMO-AMIE. *J. Geophys. Res.*, **118** (21), 11,979–
596 11,995, doi:10.1002/2013JD020421.
- 597 Powell, S. W., and R. A. Houze, 2015a: Effect of dry large-scale vertical motions on initial mjo
598 convective onset. *J. Geophys. Res.*, **120** (10), 4783–4805, doi:10.1002/2014JD022961, URL
599 <http://dx.doi.org/10.1002/2014JD022961>, 2014JD022961.

600 Powell, S. W., and R. A. Houze, 2015b: Evolution of precipitation and convective echo top heights
601 observed by TRMM radar over the indian ocean during DYNAMO. *J. Geophys. Res.*, **120** (9),
602 3906–3919, doi:10.1002/2014JD022934.

603 Qian, Y., H. Yan, L. K. Berg, S. Hagos, Z. Feng, B. Yang, and M. Huang, 2016: Assessing
604 impacts of PBL and surface layer schemes in simulating the surface-atmosphere interactions
605 and precipitation over the tropical ocean using observations from AMIE/DYNAMO. *J. Climate*,
606 **29** (22), 8191–8210, doi:10.1175/JCLI-D-16-0040.1.

607 Rowe, A. K., and R. A. Houze, Jr., 2015: Cloud organization and growth during the transition
608 from suppressed to active MJO conditions. *J. Geophys. Res.*, **120**, 10 324–10 350, doi:10.1002/
609 2014JD022948.

610 Ruppert, J. H., Jr., and R. H. Johnson, 2015: Diurnally modulated cumulus moistening in the
611 preonset stage of the Madden-Julian Oscillation during DYNAMO. *J. Atmos. Sci.*, **72**, 1622–
612 1647, doi:10.1175/JAS-D-14-0218.1.

613 Ruppert, J. H., Jr., and R. H. Johnson, 2016: On the cumulus diurnal cycle over the tropical warm
614 pool. *J. Adv. Model. Earth Syst.*, **8**, doi:10.1002/2015MS000610.

615 Saxen, T. R., and S. A. Rutledge, 1998: Surface fluxes and boundary layer recovery in TOGA
616 COARE: Sensitivity to convective organization. *J. Atmos. Sci.*, **55** (17), 2763–2781, doi:10.
617 1175/1520-0469(1998)055<2763:SFABLR>2.0.CO;2.

618 Seidel, D. J., C. O. Ao, and K. Li, 2010: Estimating climatological planetary boundary layer
619 heights from radiosonde observations: Comparison of methods and uncertainty analysis. *J. Geo-
620 phys. Res.*, **115** (D16), n/a–n/a, doi:10.1029/2009JD013680.

621 Seo, H., A. C. Subramanian, A. J. Miller, and N. R. Cavanaugh, 2014: Coupled impacts of the
622 diurnal cycle of sea surface temperature on the Madden-Julian Oscillation. *J. Climate*, **27** (22),
623 8422–8443, doi:10.1175/JCLI-D-14-00141.1.

624 Sobel, A., S. Wang, and D. Kim, 2014: Moist static energy budget of the MJO during DYNAMO.
625 *J. Atmos. Sci.*, **71** (11), 4276–4291, doi:10.1175/JAS-D-14-0052.1.

626 Soloviev, A., and R. Lukas, 1997: Observation of large diurnal warming events in the near-surface
627 layer of the western equatorial Pacific warm pool. *Deep Sea Research I*, **44**, 1055–1076, doi:
628 10.1016/S0967-0637(96)00124-0.

629 Sui, C.-H., K.-M. Lau, Y. N. Takayabu, and D. A. Short, 1997: Diurnal variations in tropical
630 oceanic cumulus convection during toga coare. *J. Atmos. Sci.*, **54** (5), 639–655, doi:10.1175/
631 1520-0469(1997)054(0639:DVITOC)2.0.CO;2.

632 Teixeira, J., and Coauthors, 2008: Parameterization of the atmospheric boundary layer: A
633 view from just above the inversion. *Bull. Amer. Meteor. Soc.*, **89** (4), 453–458, doi:10.1175/
634 BAMS-89-4-453.

635 Vialard, J., and Coauthors, 2009: Air-sea interactions in the Seychelles-Chagos Thermocline
636 Ridge region. *Bull. Amer. Meteor. Soc.*, **90**, 45–61, doi:10.1175/2008BAMS2499.2.

637 Wang, X. Y., and K. C. Wang, 2014: Estimation of atmospheric mixing layer height from ra-
638 diosonde data. *Atmos. Meas. Tech.*, **7**, 1701–1709, doi:10.5194/amt-7-1701-2014.

639 Wheeler, M. C., and H. H. Hendon, 2004: An all-season real-time multivariate MJO index: De-
640 velopment of an index for monitoring and prediction. *Mon. Wea. Rev.*, **132**, 1917–1932.

641 Xu, W., and S. A. Rutledge, 2014: Convective characteristics of the Madden-Julian Oscillation
642 over the central Indian Ocean observed by shipborne radar during DYNAMO. *J. Atmos. Sci.*,
643 **71** (8), 2859–2877, doi:10.1175/JAS-D-13-0372.1.

644 Yoneyama, K., C. Zhang, and C. N. Long, 2013: Tracking pulses of the Madden-Julian Oscillation.
645 *Bull. Amer. Meteor. Soc.*, **94**, 1871–1891, doi:10.1175/BAMS-D-12-00157.1.

646 Young, G. S., S. M. Perugini, and C. W. Fairall, 1995: Convective wakes in the equatorial west-
647 ern Pacific during TOGA. *Mon. Wea. Rev.*, **123** (1), 110–123, doi:10.1175/1520-0493(1995)
648 123<0110:CWITEW>2.0.CO;2.

649 Yuter, S. E., and R. A. Houze, Jr., 1995: Three-dimensional kinematic and microphysical evolu-
650 tion of florida cumulonimbus. part ii: Frequency distributions of vertical velocity, reflectivity,
651 and differential reflectivity. *Mon. Wea. Rev.*, **123** (7), 1941–1963, doi:10.1175/1520-0493(1995)
652 123<1941:TDKAME>2.0.CO;2.

653 Zhang, C., J. Gottschalck, E. D. Maloney, M. W. Moncrieff, F. Vitart, D. E. Waliser, B. Wang,
654 and M. C. Wheeler, 2013: Cracking the MJO nut. *Geophys. Res. Lett.*, **40**, 1223–1230, doi:
655 10.1002/grl.50244,2013.

656 Zipser, E. J., 1977: Mesoscale and convective-scale downdrafts as distinct components of squall-
657 line circulation. *Mon. Wea. Rev.*, **105**, 1568–1589, doi:10.1175/1520-0493(1977)105<1568:
658 MACDAD>2.0.CO;2.

659 Zuidema, P., and Coauthors, 2012: On trade wind cumulus cold pools. *J. Atmos. Sci.*, **69** (1),
660 258–280, doi:10.1175/JAS-D-11-0143.1.

661 **LIST OF TABLES**

662 **Table 1.** Boundary layer statistics for Gan Island for period 1 October 2011 to 8 Febru-
663 ary 2012, and Malé and R/V *Revelle* for period 1 October to 15 December
664 2011, and comparisons with TOGA COARE (Johnson et al. 2001) and GATE
665 (Fitzjarrald and Garstang 1981). Numbers in parentheses are percentages of
666 cases. Soundings with bad or missing data in ABL have been excluded from
667 the DYNAMO sounding inventory. 31

668 **Table 2.** Mean mixed layer and rainfall statistics for Gan Island, Malé, and R/V *Revelle*
669 during Special Observing Period (1 October to 15 December), and comparisons
670 with TOGA COARE (Johnson et al. 2001) and GATE (Fitzjarrald and Garstang
671 1981). Rainfall is from TRMM averaged within a 1 deg radius of each site.
672 Sigma (σ) refers to standard deviation. 32

673 TABLE 1. Boundary layer statistics for Gan Island for period 1 October 2011 to 8 February 2012, and Malé and
674 R/V *Revelle* for period 1 October to 15 December 2011, and comparisons with TOGA COARE (Johnson et al.
675 2001) and GATE (Fitzjarrald and Garstang 1981). Numbers in parentheses are percentages of cases. Soundings
676 with bad or missing data in ABL have been excluded from the DYNAMO sounding inventory.

	SOUNDING SITE					
	Gan Island	Malé	R/V <i>Revelle</i>	DYNAMO Totals	TOGA COARE	GATE
Number of sondes	1049	316	418	1783	1283	703
Mixed layer cases	726 (69.2%)	226 (71.5%)	268 (64.1%)	1220 (68.4%)	926 (72.1%)	559 (79.5%)
Stable layer cases	105 (10.0%)	36 (11.4%)	59 (14.1%)	200 (11.6%)		
Indeterminate cases	200 (19.1%)	54 (17.1%)	57 (13.6%)	311 (17.4%)		

677 TABLE 2. Mean mixed layer and rainfall statistics for Gan Island, Malé, and R/V *Revelle* during Special
678 Observing Period (1 October to 15 December), and comparisons with TOGA COARE (Johnson et al. 2001) and
679 GATE (Fitzjarrald and Garstang 1981). Rainfall is from TRMM averaged within a 1 deg radius of each site.
680 Sigma (σ) refers to standard deviation.

Station	Number	\bar{z}_i (m)	σ (m)	Skewness	z_{max}	z_{min}	Rainfall rate (mm day ⁻¹)	Rainfall frequency
Gan Island	396	503	146	-0.3	867	111	7.6	61%
Malé	226	535	171	-0.01	926	165	5.6	53%
<i>Revelle</i>	268	491	165	-0.1	914	132	9.1	65%
DYNAMO Total	890	508	158	-0.2	926	111	8.5	62%
TOGA COARE	926	512	155	0.1	961	116	8.2*	
GATE	703	424	160					

* Mean rainfall rate in Intensive Flux Array for Intensive Observing Period of TOGA COARE (Johnson and Ciesielski 2000)

681 **LIST OF FIGURES**

682 **Fig. 1.** DYNAMO enhanced sounding network for the period October-December 2011. Analyses
683 of mixed layers have been carried out on soundings from Malé (4 per day), Gan Island (8
684 per day), and *Revelle* (8 per day) (red dots), which constituted part of the northern sounding
685 array. That array experienced a stronger MJO signal than the southern array as indicated by
686 amplitude of 20-day low-pass filtered 450 hPa vertical motion (contours; hPa h^{-1} , values $>$
687 5 stippled). Colombo data were not used due to significant island influences. 35

688 **Fig. 2.** (lower) Potential temperature θ and specific humidity q profiles at 0800 and 1400 L at R/V
689 *Revelle* during a suppressed period of the MJO on 4 October 2011. Nearly well-mixed
690 profiles of θ and q extend up to approximately 500 m, surmounted by a $\sim 100\text{-m}$ deep
691 entrainment zone. Hypothesized cumulus cloud layer is depicted, topped by a trade-wind-
692 like stable layer. (upper) Terra/MODIS visible image at 1010 L indicates some scattered
693 clouds in region. Image extends from approximately 1 to 2°S and 80 to 81°E. Patchiness of
694 sea surface is a result of image occurring in sun glint. Star denotes approximate position of
695 *Revelle*. 36

696 **Fig. 3.** (upper) Sequence of potential temperature θ profiles at R/V *Revelle* from 2300 UTC 21
697 November to 1400 UTC 22 November (local times, LT, at 3-h intervals indicated along
698 θ profiles within figure). Boundary layer recovery (mixed layer tops indicated by red line
699 segments) over a 12-h period is approximated by dashed arrow. Surface θ values indicated at
700 base of each sounding. Successive soundings are separated by 3 K. (lower) Radar reflectivity
701 PPI scans from TOGA radar (out to 150 km radius) at 0729 and 1859 LT showing decrease
702 in areal coverage of precipitation systems. Reflectivity range: 20 dBZ (dark green) to 45
703 dBZ (orange). 37

704 **Fig. 4.** Histograms of mixed layer depth at Malé, Gan Island, and *Revelle* for the Special Observing
705 Period (1 October-15 December) using 5-hPa bins. Horizontal dashed lines indicate mean
706 values. Numbers of mixed layer cases and total soundings during period are in parentheses. 38

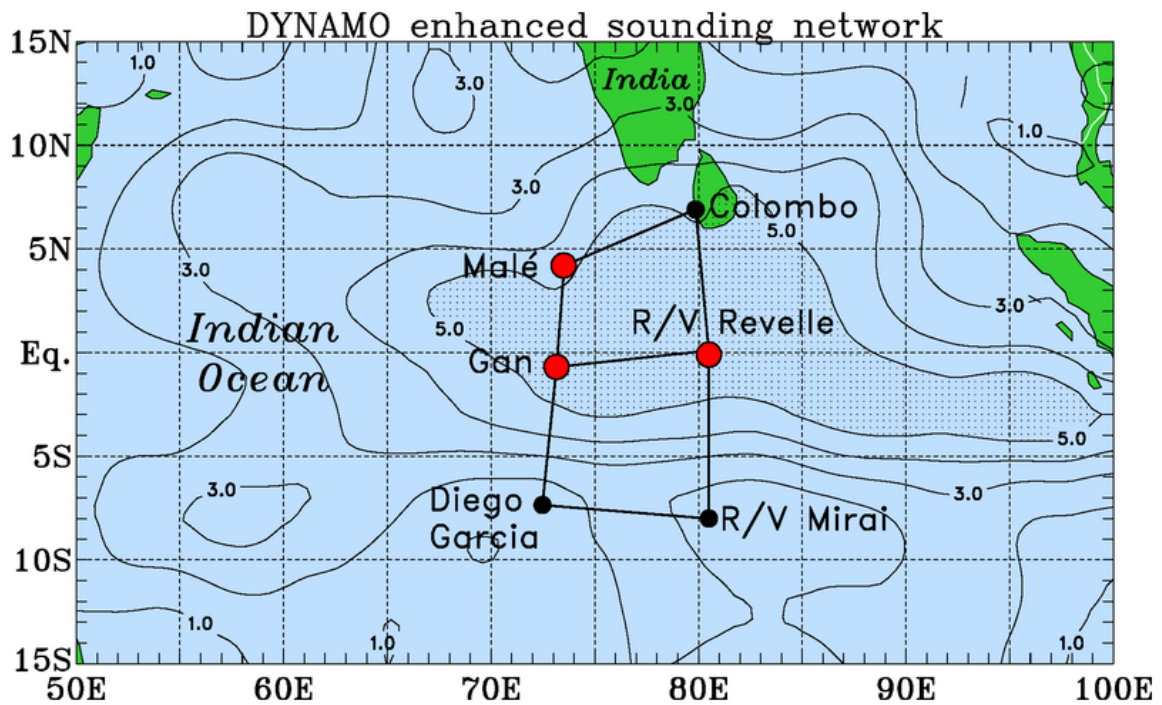
707 **Fig. 5.** Histograms of mixed layer depth at Gan Island for undisturbed (black) and disturbed (red)
708 periods for the full duration of DYNAMO (1 October 2011 to 8 February 2012) using 5-hPa
709 bins. See text for definitions. Horizontal dashed lines indicate mean values. Numbers of
710 mixed layer cases are in parentheses. 39

711 **Fig. 6.** SOP-mean profiles of wind speed $|v|$, potential temperature θ , virtual potential temperature
712 θ_v , and specific humidity q for *Revelle*, Gan, and Malé scaled by mixed layer depth. Mean
713 mixed layer depths z_i for individual sites indicated by horizontal lines. Shading at bottom
714 indicates surface effects in sounding data in lowest 50 m. Plots for all sites include only
715 those times when *Revelle* was on station at its equatorial location (3 October 08 UTC to 29
716 October 08 UTC and 10 November 20 UTC to 1 December 08 UTC). Numbers of soundings
717 indicated in parentheses. 40

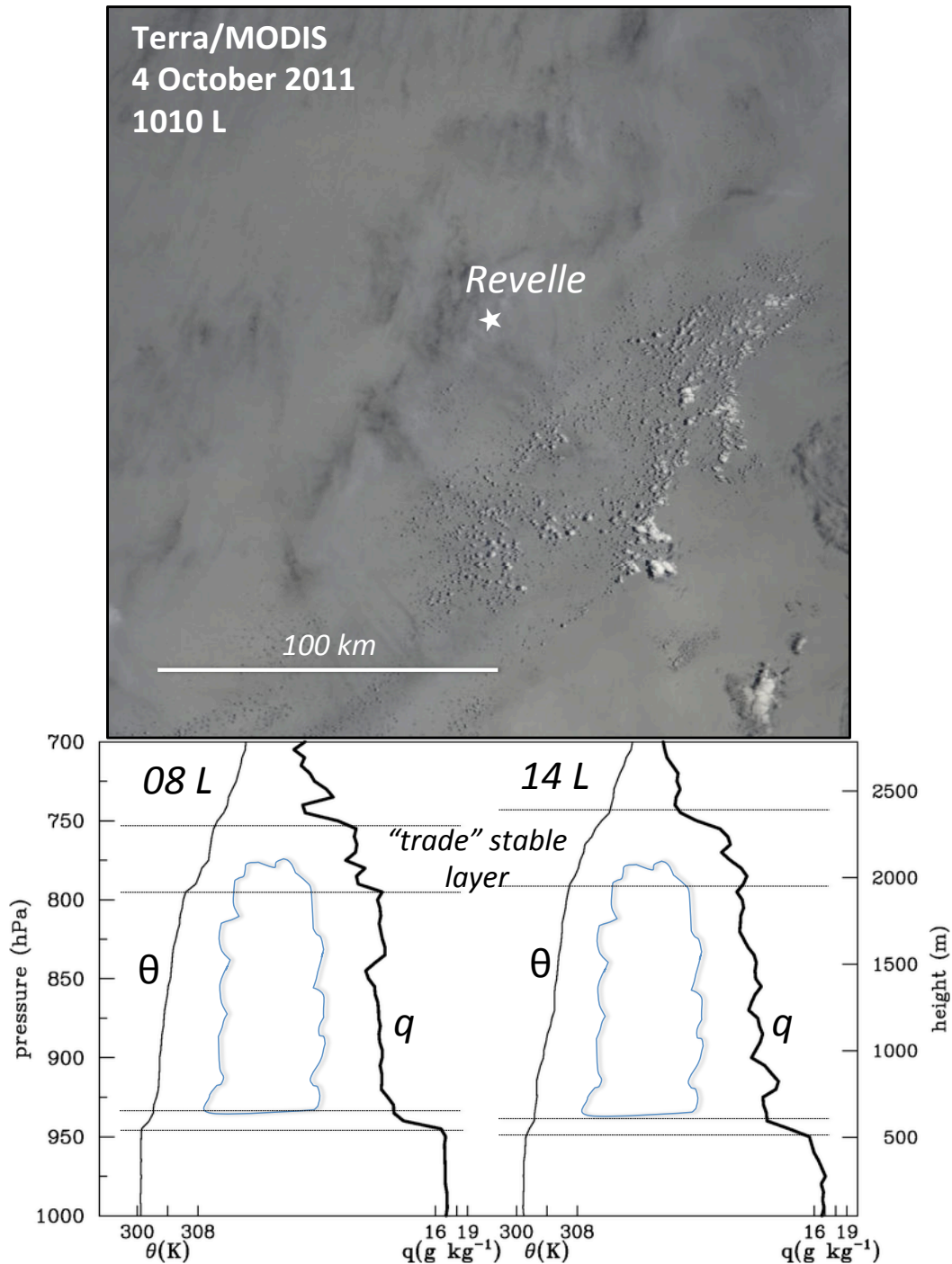
718 **Fig. 7.** CFADs of mixed-layer mean θ , q , and radar rainfall at *Revelle* for 268 mixed layer cases.
719 Vertical axis is mixed layer depth. Data have been placed into 20 bins in the horizontal and
720 8 bins in the vertical to create the CFADs. TOGA radar-estimated rainfall is for 3-h period
721 centered on sounding observation times. 41

722 **Fig. 8.** Time series of mixed layer depths (tops of red bars) at Malé, Gan, and *Revelle* for entire pe-
723 riod of DYNAMO sounding operations, black curves denote daily-averaged values. Darker
724 shaded region at bottom of panels indicates times at which soundings were taken. Daily-
725 average precipitation P_0 : from TRMM at Malé (within a 1 deg radius of the island, blue

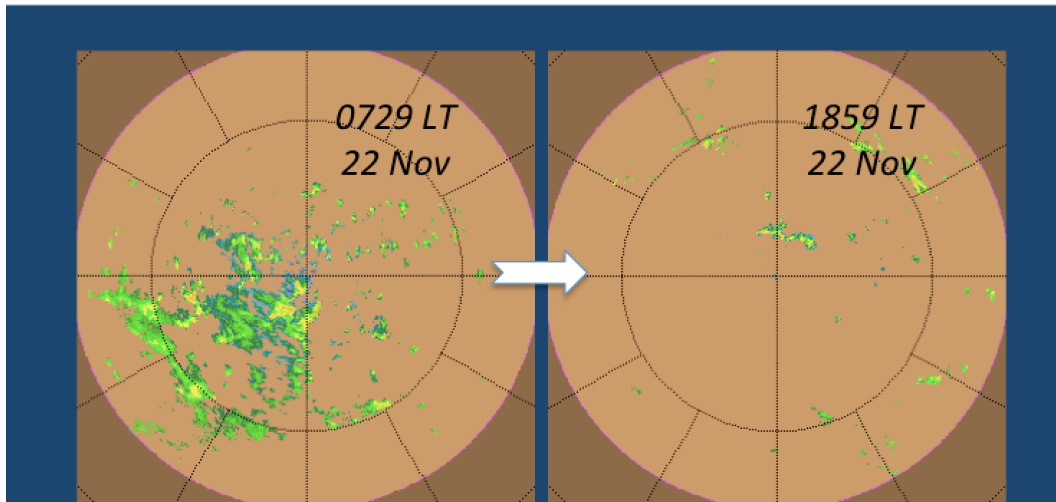
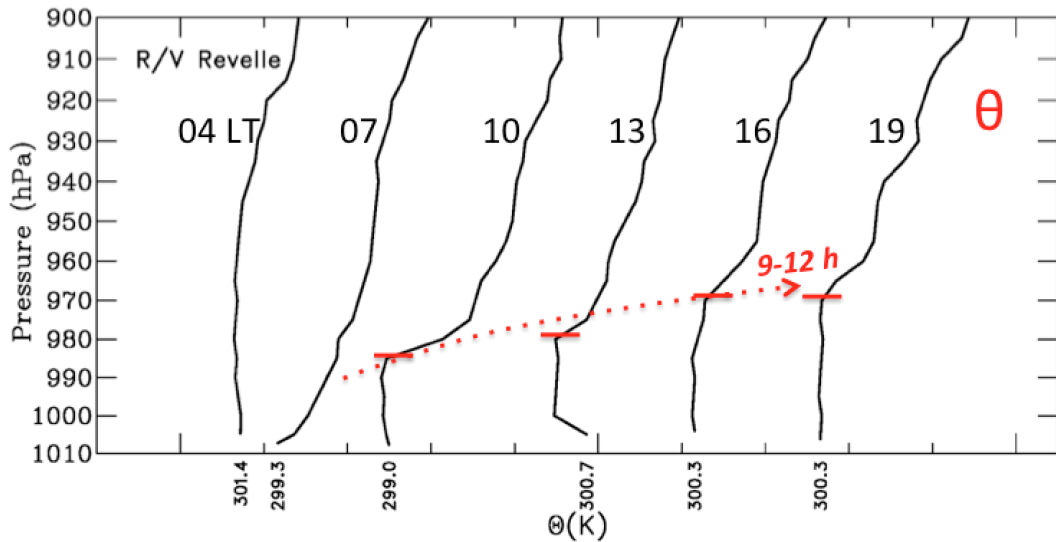
726	curve) and from radar observations at Gan and <i>Revelle</i> (green curves); precipitable water	
727	PW from the soundings (black curves). MJO phase based on Wheeler and Hendon (2004)	
728	index shown at bottom.	42
729	Fig. 9. Time series of (a) mixed layer depths (tops of black bars) during two cruises of <i>Revelle</i> (Legs	
730	2 and 3) for DYNAMO SOP along with lifting condensation level (LCL) based on mixed-	
731	layer mean conditions; (b) surface buoyancy flux F , wind speed $ v $, and surface wind plots	
732	at 6-hourly intervals; (c) SST and 19-m temperature T_{19m} ; and (d) surface relative humidity	
733	RH (adjusted to 10 m from flux tower data) and radar-estimated precipitation P_0 . All curves	
734	are daily-average values, except for z_i and SST, which are at their full measured resolution.	
735	Gray-shaded region at bottom of top panel indicates times at which soundings were taken.	
736	MJO phase based on Wheeler and Hendon (2004) index shown at bottom.	43
737	Fig. 10. Diurnal cycle of mixed layer (a) depth (m), (b) mean potential temperature (K) and (c) mean	
738	specific humidity (g kg^{-1}), and (d) <i>Revelle</i> SST for undisturbed SOP periods. Undisturbed	
739	periods definitions – Gan: 1-10 October, 11-21 November; Malé: 3-17 October; <i>Revelle</i> :	
740	11-21 November. Daytime denoted by yellow shading, local noon by sun symbol. Number	
741	of mixed layer cases are in parentheses.	44
742	Fig. 11. Diurnal cycle of (a) surface temperature (C), (b) surface specific humidity (g kg^{-1}), and (c)	
743	surface relative humidity (%) for undisturbed periods at Gan, Malé, and <i>Revelle</i> . Surface	
744	measurements at <i>Revelle</i> were at 19 m, those at Gan and Malé were at shelter height of 2 m.	
745	Rest as in Fig. 10.	45
746	Fig. 12. Mean diurnal cycle of specific humidity q (g kg^{-1}), potential temperature θ , and wind speed	
747	(m s^{-1}) for 11-21 November undisturbed period at <i>Revelle</i> . Variables in each sounding are	
748	first scaled by mixed layer depth z_i , then composited according to height relative to z_i , and	
749	finally replotted as a function of actual height z . Mixed-layer top z_i (black curve) is shown.	
750	Values in lowest 50 m are shaded to indicate surface effects in sounding data.	46
751	Fig. 13. (a) Diurnal cycle of mixed layer depth z_i (m) and lifting condensation level (LCL) based on	
752	mixed-layer mean conditions, (b) mean radar-determined rainfall rate P_0 (green) in TOGA	
753	radar range and ceilometer-estimated cloud cover (cloud symbols), and (c) mean SST (blue)	
754	and surface buoyancy flux F (red) for November undisturbed period at <i>Revelle</i> . Gray shading	
755	indicates difference between LCL and z_i . Diurnal cycle range and mean value of z_i , along	
756	with numbers of soundings at each time (on bottom axis), are shown in top panel.	47
757	Fig. 14. Diurnal time-height composites of convective echo-top frequency (shading; %) and echo	
758	area coverage (solid black line; %; right axis) for 13-16 November suppressed period, cal-	
759	culated from 15-min S-PolKa RHI data. Local time is indicated along the abscissa. Red	
760	asterisk marks the time of increasing echo-top frequency and echo area coverage. Horizontal	
761	dashed line indicates the 0°C level. Adapted from Ruppert and Johnson (2015).	48



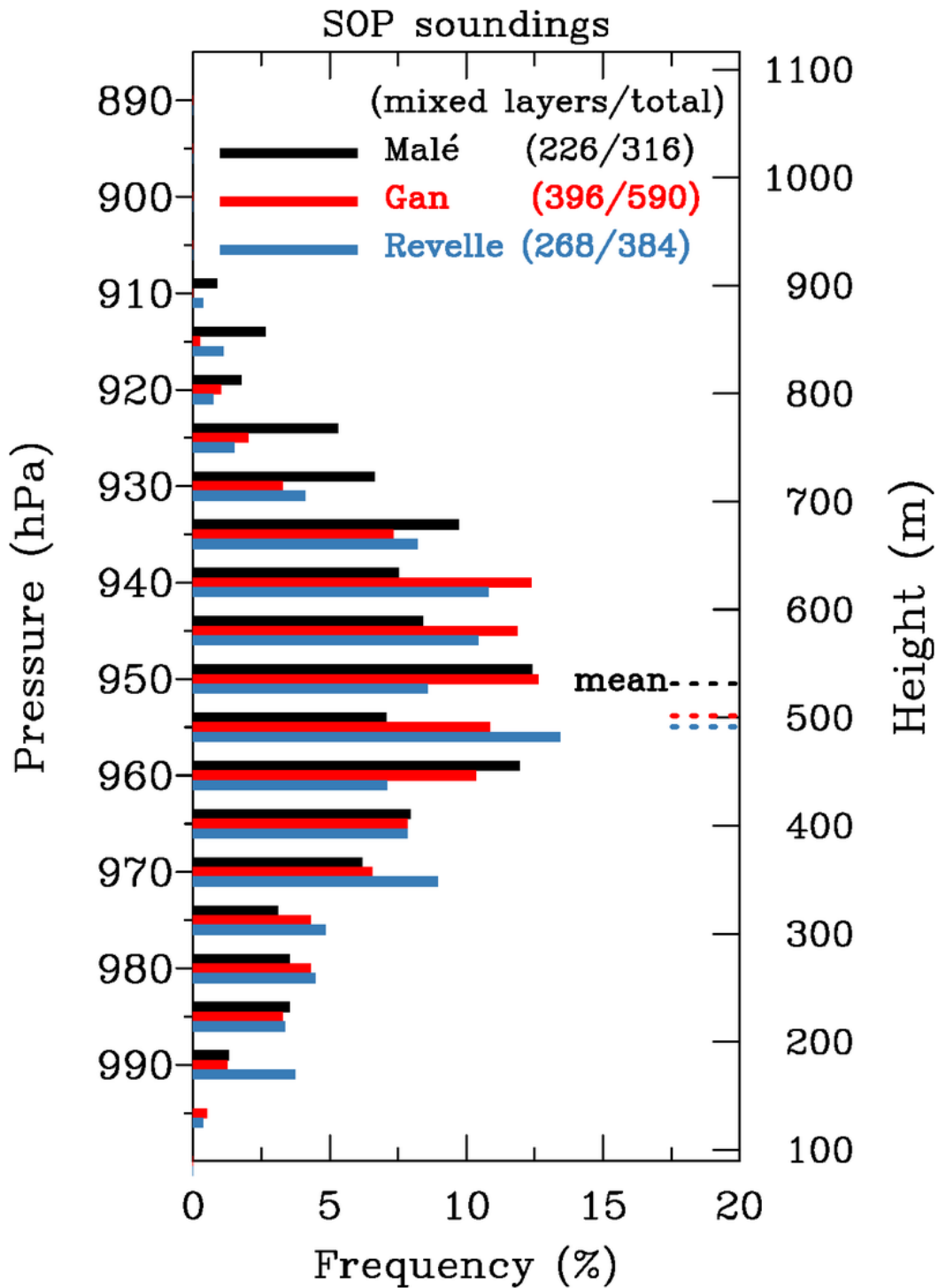
762 FIG. 1. DYNAMO enhanced sounding network for the period October-December 2011. Analyses of mixed
 763 layers have been carried out on soundings from Malé (4 per day), Gan Island (8 per day), and *Revelle* (8 per day)
 764 (red dots), which constituted part of the northern sounding array. That array experienced a stronger MJO signal
 765 than the southern array as indicated by amplitude of 20-day low-pass filtered 450 hPa vertical motion (contours;
 766 hPa h^{-1} , values > 5 stippled). Colombo data were not used due to significant island influences.



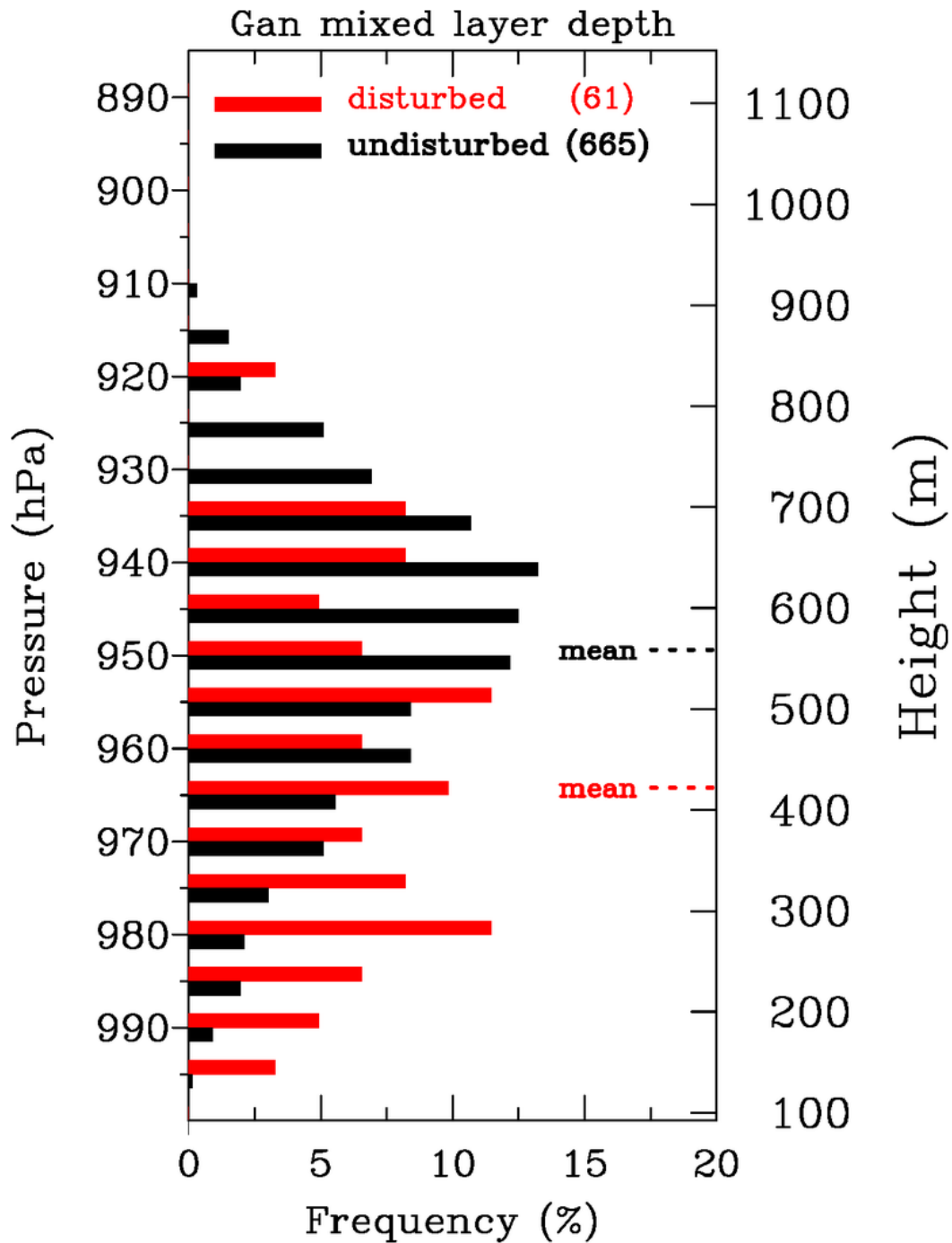
767 FIG. 2. (lower) Potential temperature θ and specific humidity q profiles at 0800 and 1400 L at R/V *Revelle*
 768 during a suppressed period of the MJO on 4 October 2011. Nearly well-mixed profiles of θ and q extend up to
 769 approximately 500 m, surmounted by a ~ 100 -m deep entrainment zone. Hypothesized cumulus cloud layer is
 770 depicted, topped by a trade-wind-like stable layer. (upper) Terra/MODIS visible image at 1010 L indicates some
 771 scattered clouds in region. Image extends from approximately 1 to 2°S and 80 to 81°E. Patchiness of sea surface
 772 is a result of image occurring in sun glint. Star denotes approximate position of *Revelle*.



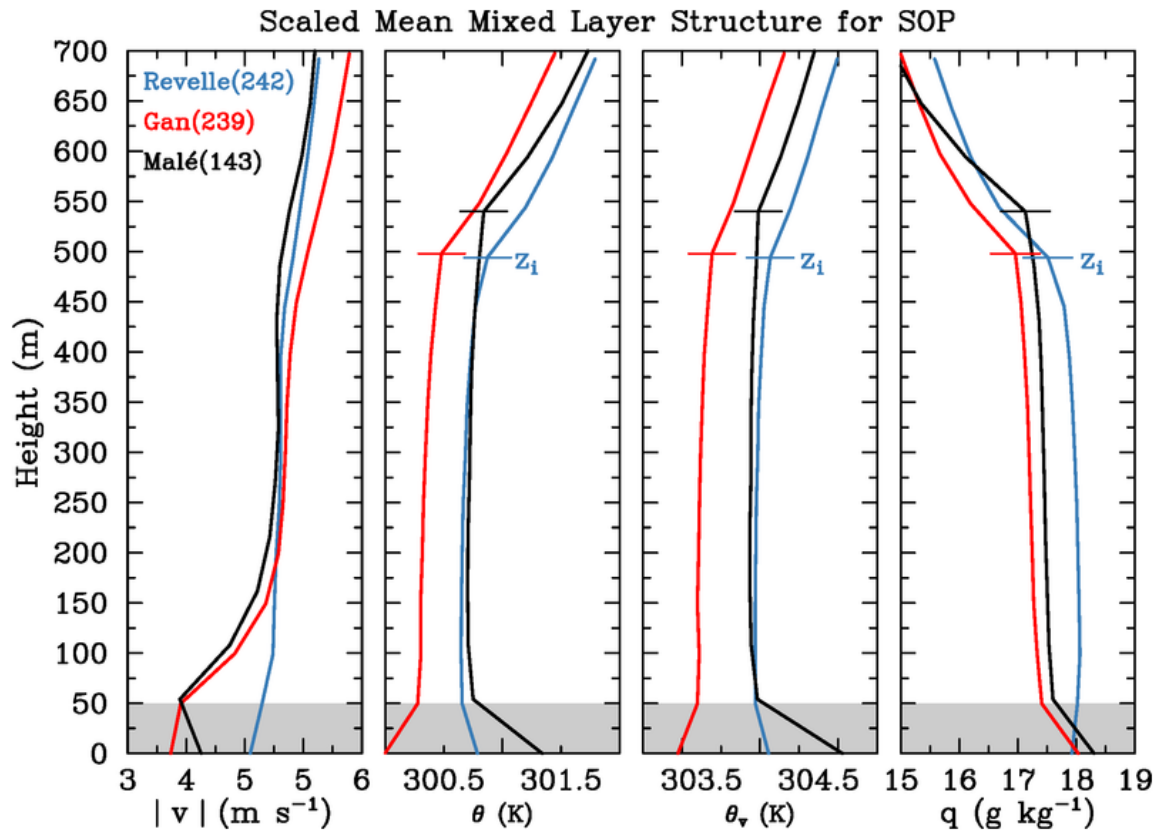
773 FIG. 3. (upper) Sequence of potential temperature θ profiles at R/V *Revelle* from 2300 UTC 21 November to
 774 1400 UTC 22 November (local times, LT, at 3-h intervals indicated along θ profiles within figure). Boundary
 775 layer recovery (mixed layer tops indicated by red line segments) over a 12-h period is approximated by dashed
 776 arrow. Surface θ values indicated at base of each sounding. Successive soundings are separated by 3 K. (lower)
 777 Radar reflectivity PPI scans from TOGA radar (out to 150 km radius) at 0729 and 1859 LT showing decrease in
 778 areal coverage of precipitation systems. Reflectivity range: 20 dBZ (dark green) to 45 dBZ (orange).



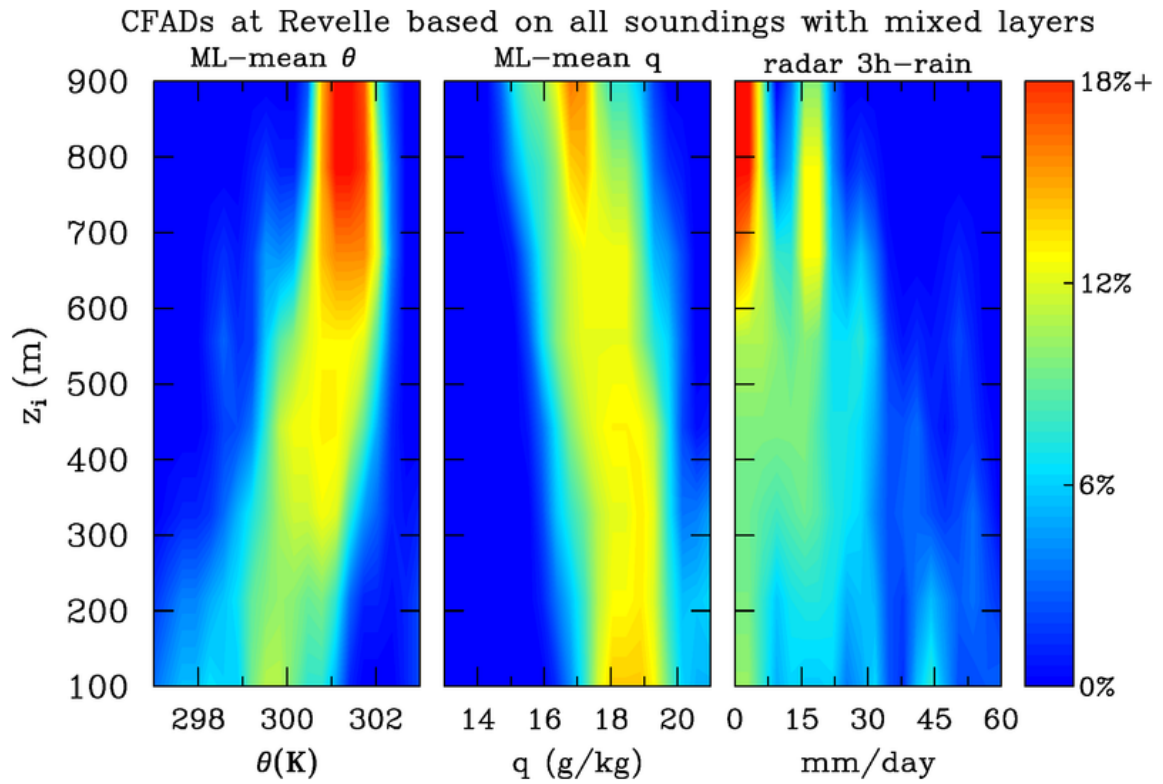
779 FIG. 4. Histograms of mixed layer depth at Malé, Gan Island, and *Revelle* for the Special Observing Period
 780 (1 October-15 December) using 5-hPa bins. Horizontal dashed lines indicate mean values. Numbers of mixed
 781 layer cases and total soundings during period are in parentheses.



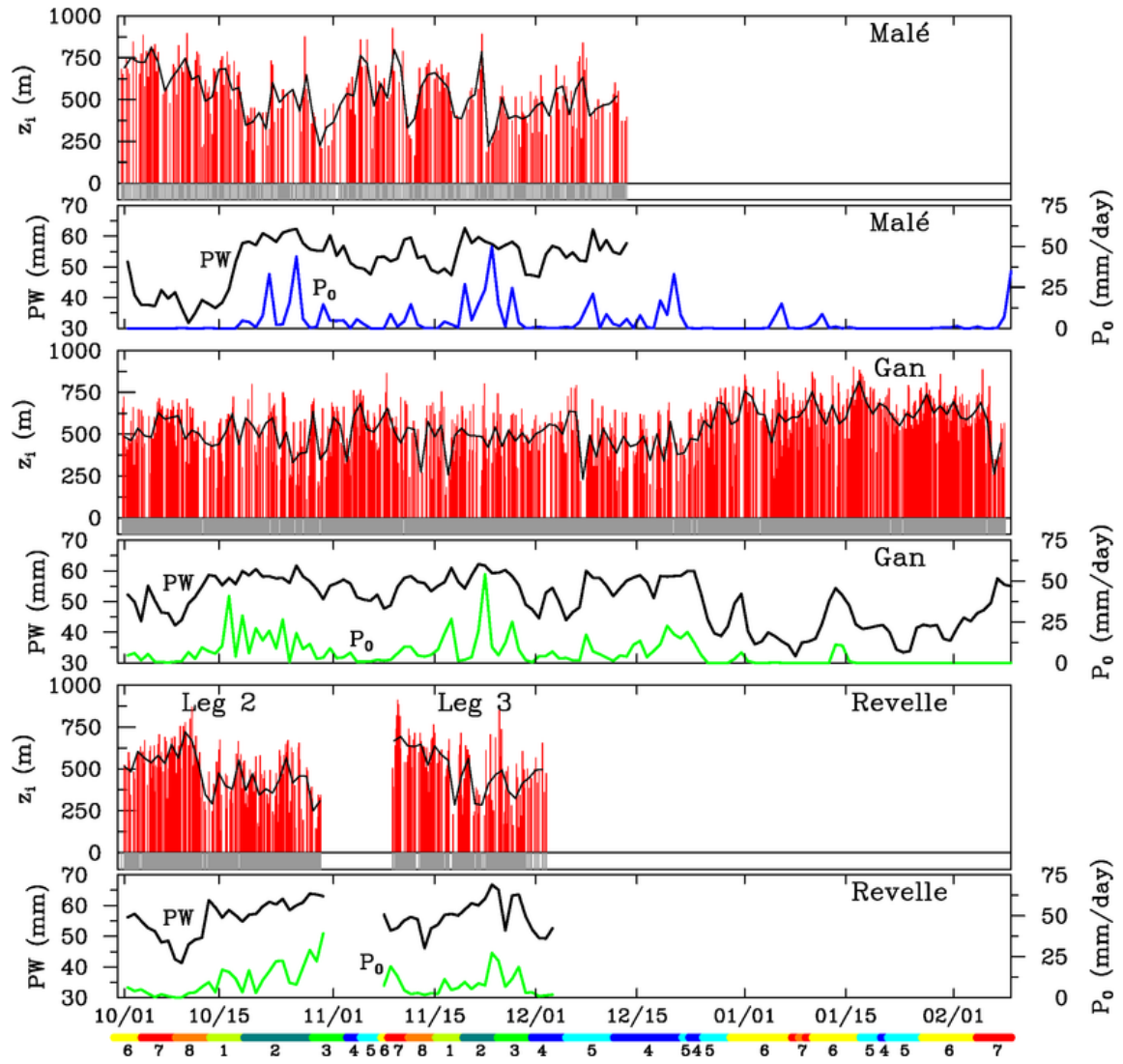
782 FIG. 5. Histograms of mixed layer depth at Gan Island for undisturbed (black) and disturbed (red) periods for
 783 the full duration of DYNAMO (1 October 2011 to 8 February 2012) using 5-hPa bins. See text for definitions.
 784 Horizontal dashed lines indicate mean values. Numbers of mixed layer cases are in parentheses.



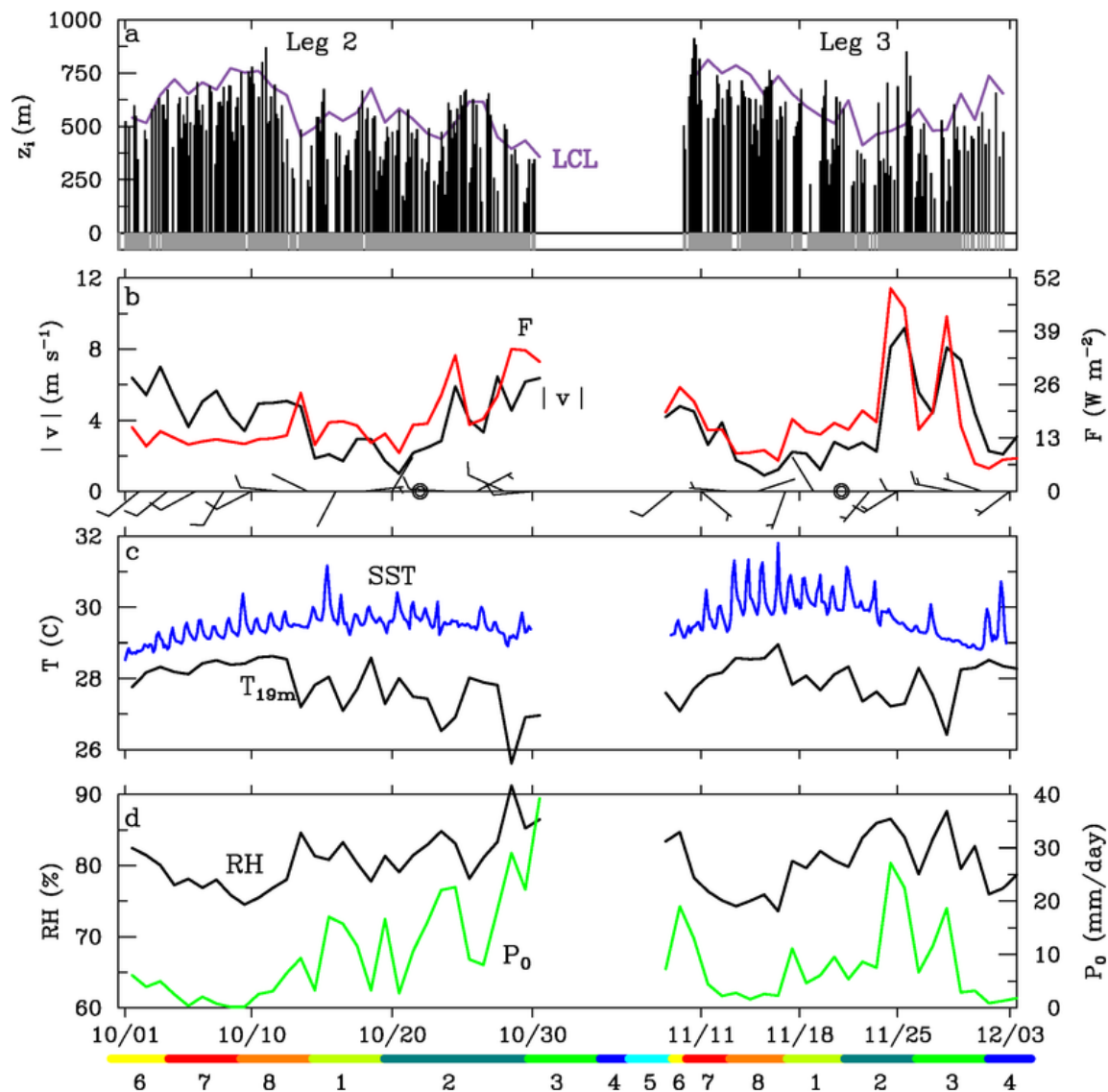
785 FIG. 6. SOP-mean profiles of wind speed $|v|$, potential temperature θ , virtual potential temperature θ_v , and
 786 specific humidity q for *Reville*, *Gan*, and *Malé* scaled by mixed layer depth. Mean mixed layer depths z_i for
 787 individual sites indicated by horizontal lines. Shading at bottom indicates surface effects in sounding data in
 788 lowest 50 m. Plots for all sites include only those times when *Reville* was on station at its equatorial location
 789 (3 October 08 UTC to 29 October 08 UTC and 10 November 20 UTC to 1 December 08 UTC). Numbers of
 790 soundings indicated in parentheses.



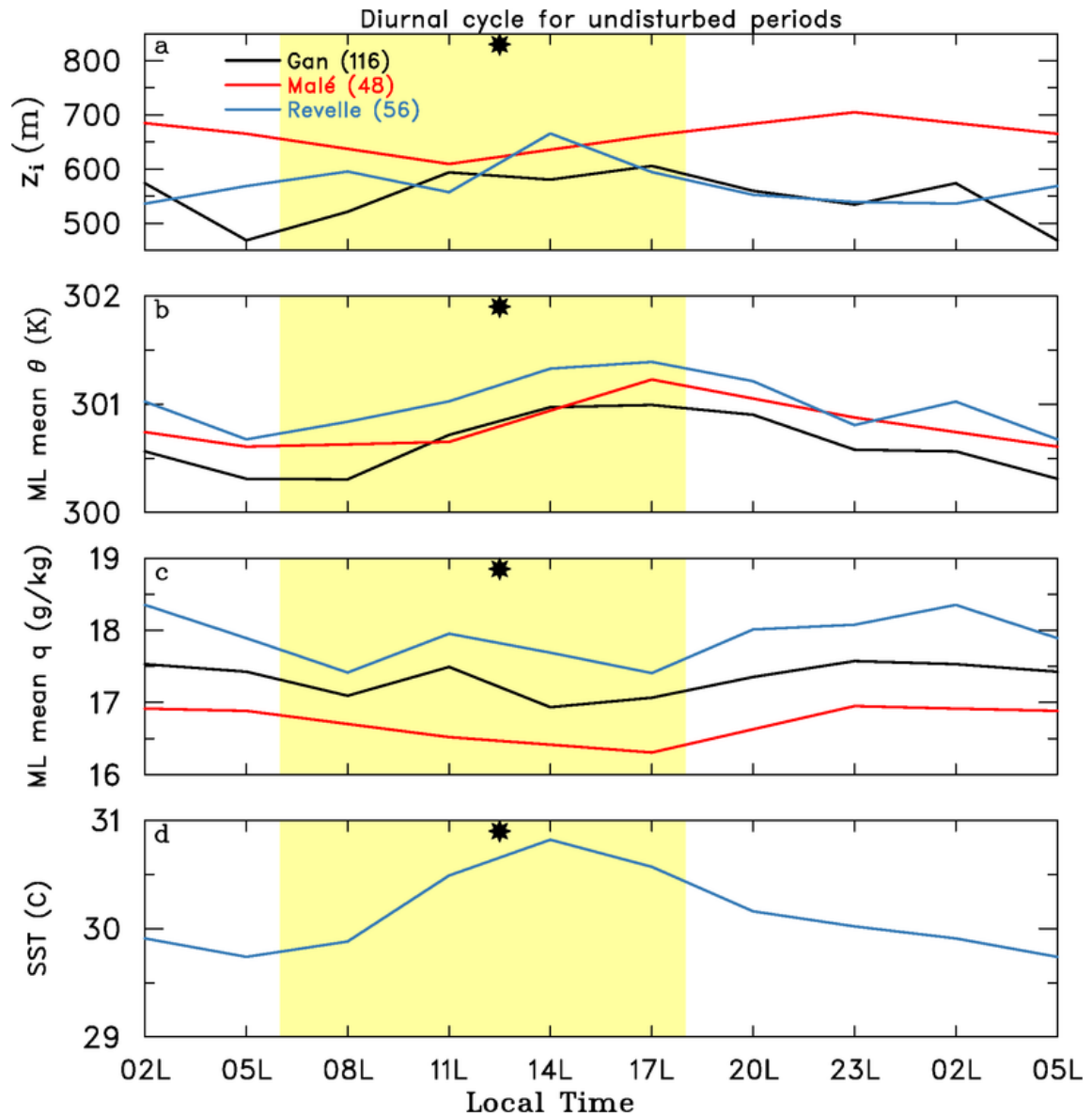
791 FIG. 7. CFADs of mixed-layer mean θ , q , and radar rainfall at *Revelle* for 268 mixed layer cases. Vertical
 792 axis is mixed layer depth. Data have been placed into 20 bins in the horizontal and 8 bins in the vertical to create
 793 the CFADs. TOGA radar-estimated rainfall is for 3-h period centered on sounding observation times.



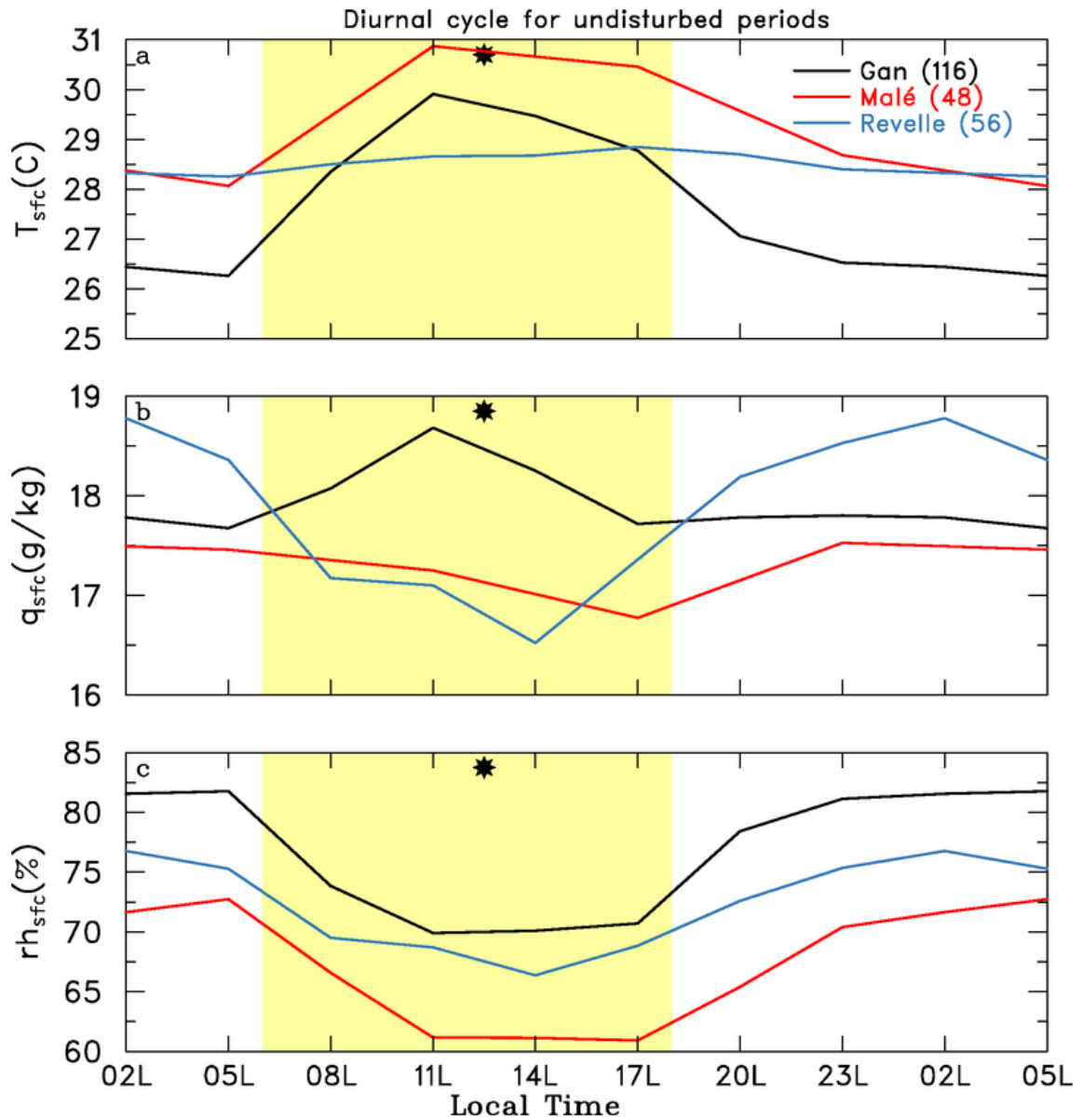
794 FIG. 8. Time series of mixed layer depths (tops of red bars) at Malé, Gan, and *Revelle* for entire period of
 795 DYNAMO sounding operations, black curves denote daily-averaged values. Darker shaded region at bottom of
 796 panels indicates times at which soundings were taken. Daily-average precipitation P_0 : from TRMM at Malé
 797 (within a 1 deg radius of the island, blue curve) and from radar observations at Gan and *Revelle* (green curves);
 798 precipitable water PW from the soundings (black curves). MJO phase based on Wheeler and Hendon (2004)
 799 index shown at bottom.



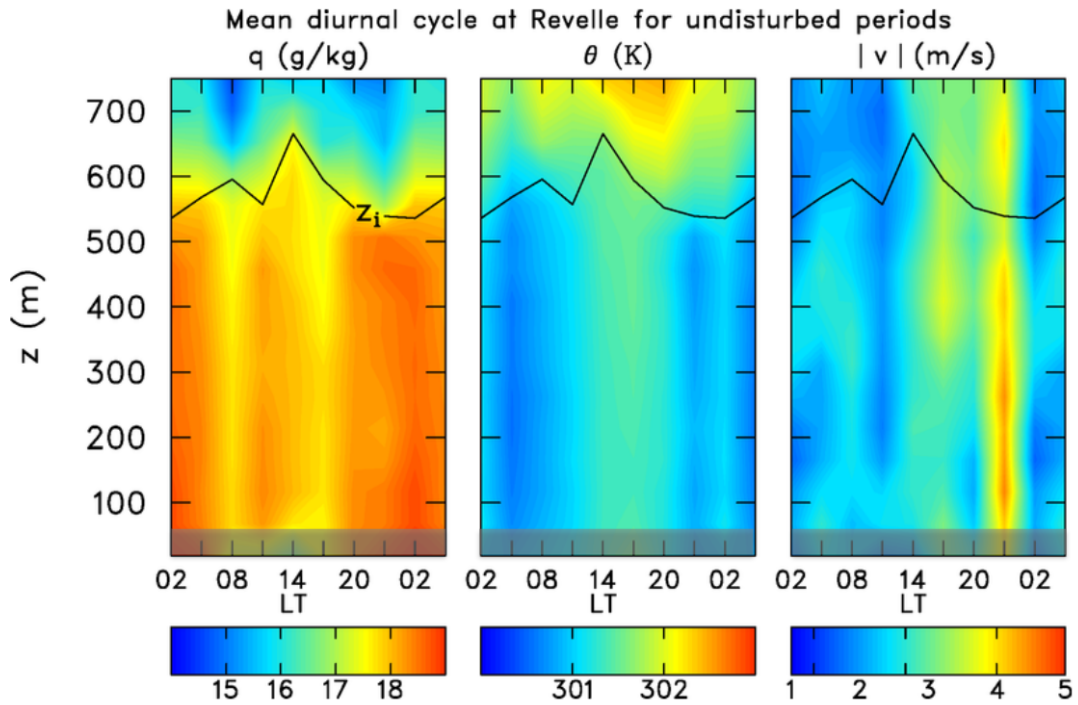
800 FIG. 9. Time series of (a) mixed layer depths (tops of black bars) during two cruises of *Revelle* (Legs 2
 801 and 3) for DYNAMO SOP along with lifting condensation level (LCL) based on mixed-layer mean conditions;
 802 (b) surface buoyancy flux F , wind speed $|v|$, and surface wind plots at 6-hourly intervals; (c) SST and 19-m
 803 temperature T_{19m} ; and (d) surface relative humidity RH (adjusted to 10 m from flux tower data) and radar-
 804 estimated precipitation P_0 . All curves are daily-average values, except for z_i and SST, which are at their full
 805 measured resolution. Gray-shaded region at bottom of top panel indicates times at which soundings were taken.
 806 MJO phase based on Wheeler and Hendon (2004) index shown at bottom.



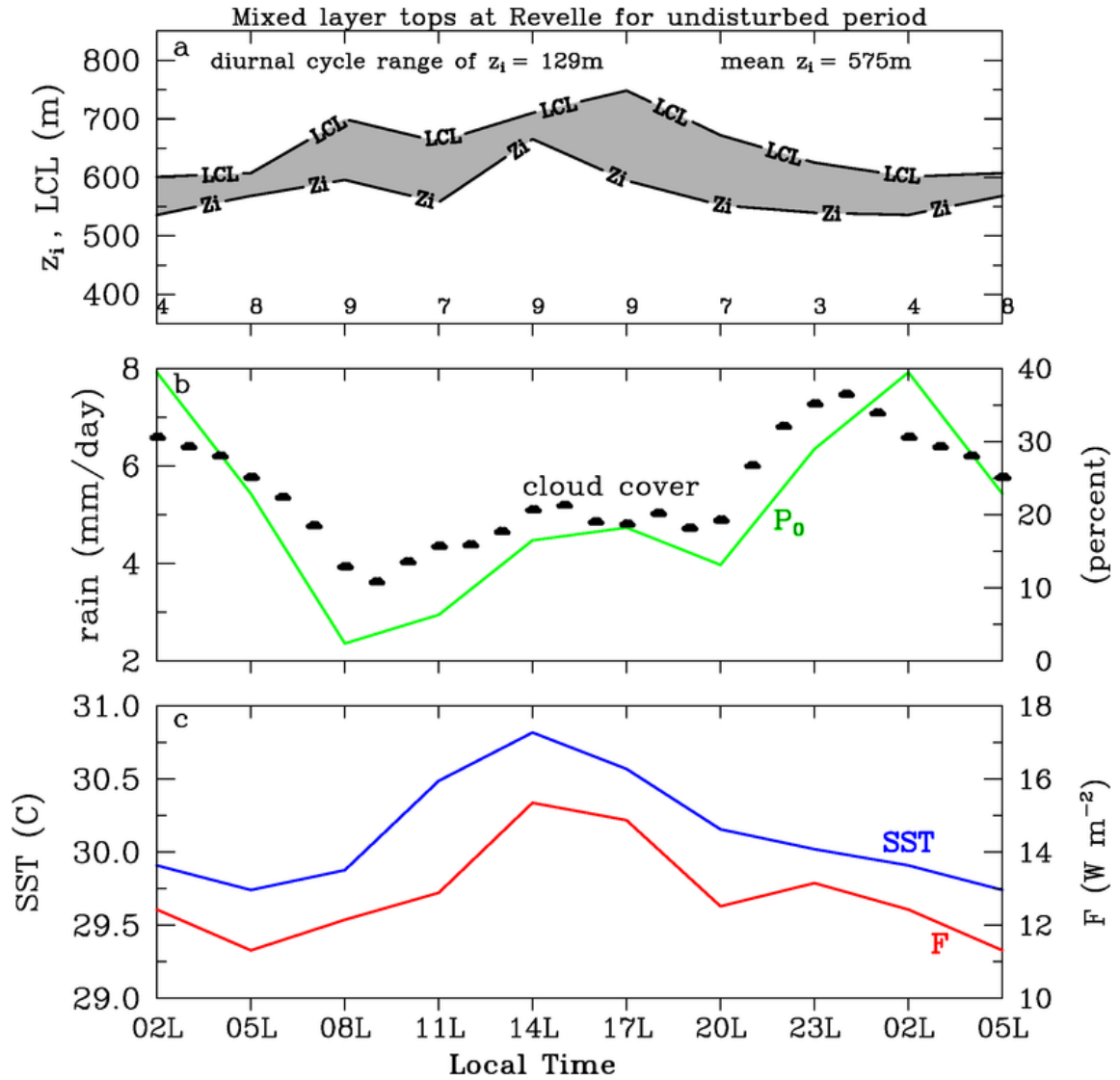
807 FIG. 10. Diurnal cycle of mixed layer (a) depth (m), (b) mean potential temperature (K) and (c) mean specific
 808 humidity (g kg^{-1}), and (d) *Revelle* SST for undisturbed SOP periods. Undisturbed periods definitions – Gan:
 809 1-10 October, 11-21 November; Malé: 3-17 October; *Revelle*: 11-21 November. Daytime denoted by yellow
 810 shading, local noon by sun symbol. Number of mixed layer cases are in parentheses.



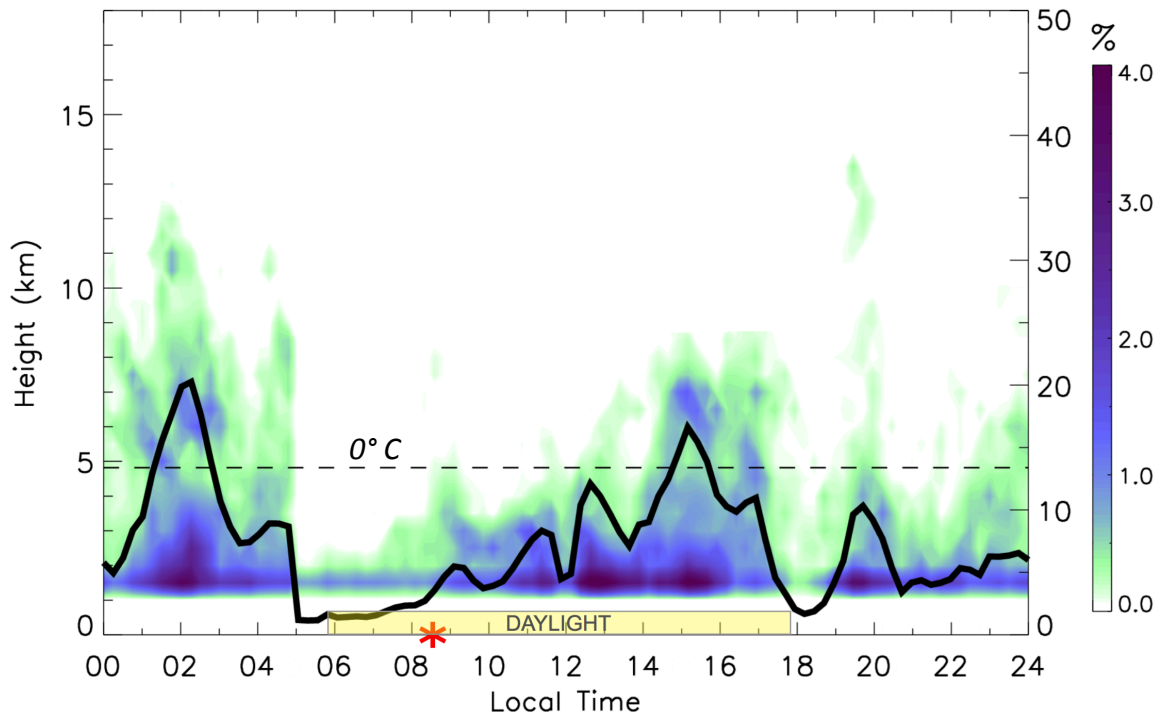
811 FIG. 11. Diurnal cycle of (a) surface temperature ($^{\circ}\text{C}$), (b) surface specific humidity (g kg^{-1}), and (c) surface
 812 relative humidity (%) for undisturbed periods at Gan, Malé, and *Reville*. Surface measurements at *Reville* were
 813 at 19 m, those at Gan and Malé were at shelter height of 2 m. Rest as in Fig. 10.



814 FIG. 12. Mean diurnal cycle of specific humidity q (g kg^{-1}), potential temperature θ , and wind speed (m s^{-1})
 815 for 11-21 November undisturbed period at *Reville*. Variables in each sounding are first scaled by mixed layer
 816 depth z_i , then composited according to height relative to z_i , and finally replotted as a function of actual height
 817 z . Mixed-layer top z_i (black curve) is shown. Values in lowest 50 m are shaded to indicate surface effects in
 818 sounding data.



819 FIG. 13. (a) Diurnal cycle of mixed layer depth z_i (m) and lifting condensation level (LCL) based on mixed-
 820 layer mean conditions, (b) mean radar-determined rainfall rate P_0 (green) in TOGA radar range and ceilometer-
 821 estimated cloud cover (cloud symbols), and (c) mean SST (blue) and surface buoyancy flux F (red) for November
 822 undisturbed period at *Reville*. Gray shading indicates difference between LCL and z_i . Diurnal cycle range and
 823 mean value of z_i , along with numbers of soundings at each time (on bottom axis), are shown in top panel.



824 FIG. 14. Diurnal time-height composites of convective echo-top frequency (shading; %) and echo area cov-
 825 erage (solid black line; %; right axis) for 13-16 November suppressed period, calculated from 15-min S-PolKa
 826 RHI data. Local time is indicated along the abscissa. Red asterisk marks the time of increasing echo-top fre-
 827 quency and echo area coverage. Horizontal dashed line indicates the 0°C level. Adapted from Ruppert and
 828 Johnson (2015).